AD-766 945

NEAR FIELD SMALL EARTHQUAKE SOURCE SPECTRA

Charles B. Archambeau, et al

California Institute of Technology

Prepared for:

Air Force Office of Scientific Research
Advanced Research Projects Agency

August 1973

California Institute of Technology
Division of Geological and Planetary Sciences
Seismological Laboratory
Pasadena, California 91109

ANNUAL REPORT

1 June 1972 - 31 May 1973

ARPA Order No:	2134
Program Code:	2F10
Contractor:	California Institute of Technology
Effective Date of Contract:	1 June 1972
Contract Expiration Date:	31 May 1973
Amount of Contract:	$99,562
Contract Number:	F44620-72-C-0083
Principal Investigators:	Charles B. Archambeau Donald V. Helmberger (213) 795-8806
Program Manager:	William J. Best (202 694-5456
Title:	Near Field Small Earthquake Source Spectra

Sponsored by
Advanced Research Projects Agency
ARPA Order No. 2134

NCLASSIFIED
Security Classification

DOCUMENT CONTROL DATA - R & D

(Security classification of title, body of abstract and indexing annotation must be entered when the overall report is classified)

1. ORIGINATING ACTIVITY (Corporate author)	2a. REPORT SECURITY CLASSIFICATION
California Institute of Technology Division of Geological and Planetary Sciences Pasadena, CA 91109	Unclassified
	2b. GROUP

3. REPORT TITLE

Near Field Small Earthquake Source Spectra

4. DESCRIPTIVE NOTES (Type of report and inclusive dates)

Scientific.....Interim (Annual Report 1 Jun 72 - 31 May 73)

5. AUTHOR(S) (First name, middle initial, last name)

Charles B. Archambeau and Donald V. Helmberger

6. REPORT DATE	7a. TOTAL NO. OF PAGES	7b. NO. OF REFS
August 1973	~~69~~ 73	0

8a. CONTRACT OR GRANT NO.	9a. ORIGINATOR'S REPORT NUMBER(S)
F44620-72-C-0083	
b. PROJECT NO. AO 2134	
c. 62701D	9b. OTHER REPORT NO(S) (Any other numbers that may be assigned this report) AFOSR - TR - 73 - 1597
d.	

10. DISTRIBUTION STATEMENT

Approved for public release; distribution unlimited.

11. SUPPLEMENTARY NOTES	12. SPONSORING MILITARY ACTIVITY
TECH, OTHER	AF Office of Scientific Research/NPG 1400 Wilson Boulevard Arlington, VA 22209

13. ABSTRACT

The present report describes research accomplished during the first year of the cooperative program aimed at determining the nature of the seismic radiation from small strike-slip earthquakes. Our activities have been in two areas, to develop and operate four long period portable stations in the area to be monitored, and to develop the necessary theoretical framework for the interpretation of the observational data.

DD FORM 1 NOV 65 1473

UNCLASSIFIED
Security Classification

Security Classification

14. KEY WORDS	LINK A		LINK B		LINK C	
	ROLE	WT	ROLE	WT	ROLE	WT
Seismic Radiation Small Strike-Slip Earthquakes long period portable stations						

Security Classification

TABLE OF CONTENTS

ABSTRACT

The present report describes research accomplished during the first year of the cooperative program aimed at determining the nature of the seismic radiation from small strike-slip earthquakes. Our activities have been in two areas, to develop and operate four long period portable stations in the area to be monitored, and to develop the necessary theoretical framework for the interpretation of the observational data.

In summary, during the first year contract period we: (1) developed four, low power multi-component long period trailer units with broadband recording capability employing both analog and digital recording capability (7 channels each); (2) upgraded eight existing trailer units to broadband, analog recording capability to record both long and short period data; (3) installed and operated a four trailer array in Bear Valley, California area and successfully recorded two small events (magnitudes 4 and 3.5) from Bear Valley and numerous teleseismic events; (4) investigated near and far field radiation from relaxation source models of earthquakes and extended the theory to a variety of source geometries and prestress conditions. It was found that the low frequency behavior of the near field was 1/f, as expected. The low frequency behavior of the far field varies between a flat spectrum and a spectrum decreasing as f^2 with decreasing frequency away from a spectral peak, depending on whether the prestress field is uniform to infinity or concentrated in a zone of characteristic dimension equal to a few times the

fault dimension. Larger, yet finite, prestress zones produce a broad spectral peak, the spectrum remaining nearly flat with decreasing frequency to a characteristic frequency which is controlled by the dimension of the prestress zone, below which the spectrum begins to decrease again as f^2 for lower frequencies. Within a wavelength or so from the source the spectrum is dominated by the near field spectral component. At high frequencies, above the characteristic "peak" or "corner" frequency determined by the rupture length and rupture velocity, the spectrum decreases as 1/3.; (5) investigated near field wave propagation in a layered medium using the Cagnaird method incorporating various simple source models and applied the method to the prediction of the field from several small earthquakes, with reasonable first order agreement with observations; (6) incorporated complex source models (e.g., relaxation and dislocation types) in surface and body wave (ray theoretic) programs. Both near and far field source terms are included and these computations should be accurate in the teleseismic and intermediate distance ranges (up to a wavelength or two from the source). The programs are being used to predict m_b and M_s from earthquakes. Preliminary results for m_b vs. M_s are in overall agreement with observations. A cutoff m_b value is predicted implying that if 1 cps energy is used to calculate m_b, then the maximum m_b for any earthquake, however large, will be about 7.0, and for "normal" prestress levels of a few hundred bars, the maximum m_b will be near 6.0. An M_S cutoff value of around 10 to 11 is also predicted.

I. Introduction

The purpose of the research conducted under this contract is to determine the detailed nature of the seismic radiation spectrum from small earthquakes, especially the nature of the long period part of the spectrum. The objective is to not only verify discrimination criteria for various types of small earthquakes (e.g., m_b vs. M_s criteria) but to obtain a fundamental understanding of why such criteria work. This implies that we must obtain a model for an earthquake that is sophisticated, incorporating the basic physics of the process, and, in addition, that we must be able to predict the near field wave propagation effects as well as far field wave propagation in order to interpret the observations in terms of the earthquake model.

Our work under this contract during the first year has therefore been divided into: (1) Field operations and instrumental systems fabrication. (2) Investigations of wave propagation theory from complex seismic sources in the near and far field distance ranges. And (3) Modeling of earthquake by numerical and analytical relaxation sources.

In addition, of course, data reduction and interpretation would be an essential part of our program; however no well recorded earthquake was obtained during the present contract period, so that no extensive interpretive work was done. Hopefully we will have the opportunity to analyze an earthquake from the Bear Valley area during the course of the next contract period.

In the following sections we discuss our accomplishments in some detail, with many of the theoretical results incorporated in this report

prior to publication in order that other program investigators be aware of the implications of our work in their own investigations.

II. Field Program and Instrumentation

Our part of the cooperative field program was to provide recording of the long period radiation from small earthquakes in the magnitude range 3.0 to 5.0. Four systems were to be designed and placed in the designated field site near Bear Valley, California. In this section we describe the system design used to achieve broad band recording in the range from a few cycles out to periods of around 60 seconds, as well as the field program actually undertaken in cooperation with other investigators.

(1) Instrumental Characteristics of Mark I and Mark II Trailer Units

In order to achieve a highly portable and reliable field recording system for long period seismic radiation from small events, we chose to employ internally recording trailer units, using a relatively short period seismometer (with adjustable period from 5 to 15 sec) in order to avoid drift problems associated with longer period seismometers. Furthermore, use of the 5 sec seismometer minimizes parasitic effects inherent in long period recording, wherein high frequency pulses result in nonlinear response producing long period motion of the recorder. In order to extend the useful response of the system to long periods, we apply a variety of high frequency filtering followed by amplification of the low frequency output using very low noise amplifiers.

Two separate trailer systems are employed in the present program, both of them are self contained recording systems with their own battery and/or solar power available if necessary. The newest (Mark II) units, constructed under the present program, record both digitally and in analog form with a rather wide variety of filter settings available, resulting in both long period and short period recording capability. The digital recording is used for the long period data, and with a sample rate of 2 samples/sec will record seven channels of data for approximately 8 days before a tape replacement is necessary. Two different filter settings can be used, or two different gain levels can be recorded. The analog recording can be carried on simultaneously and can be used for either high or low frequency recording (using variable filtering) of the 5 sec seismometer output or it can be used to simultaneously record data from a different type of seismometer. The analog system records over a 40 db range.

Since the construction of the new Mark II units was in progress over much of the current report period, we employed four of our older (Mark I) trailer units as recorders in the field over this period. We have eight such units, all of which record on FM magnetic tape and on film. We modified all eight units to function as broad band systems, and in particular, when using the 5 sec seismometers, the system response is very close to the long period response of the Mark II units. These units will be replaced in the field by the new Mark II systems as they become available. At this time the Mark II units are complete and are being field tested, so that replacement should begin soon. (One or two of the

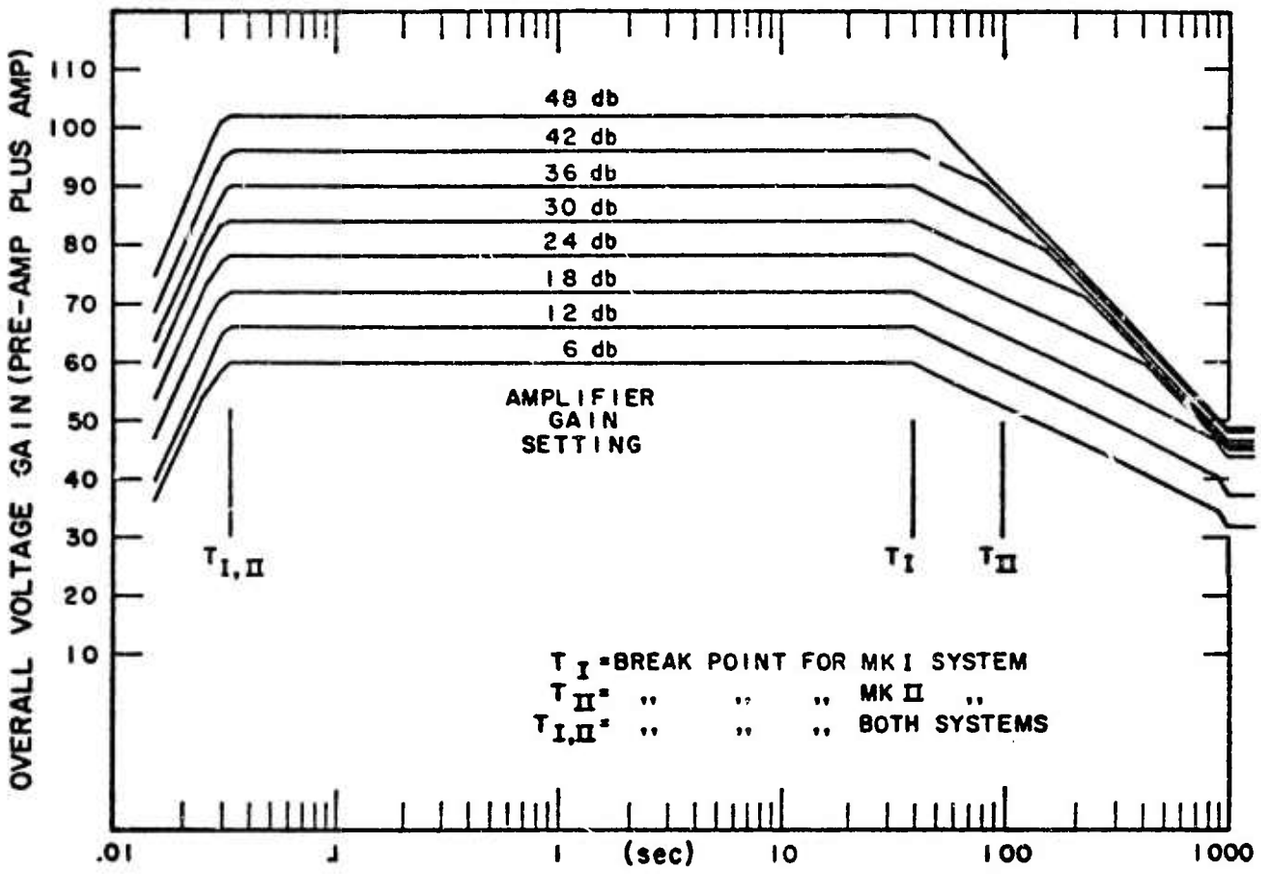

MARK I & II TRAILER SYSTEM AMPLIFIER PASS BANDS

Figure 1

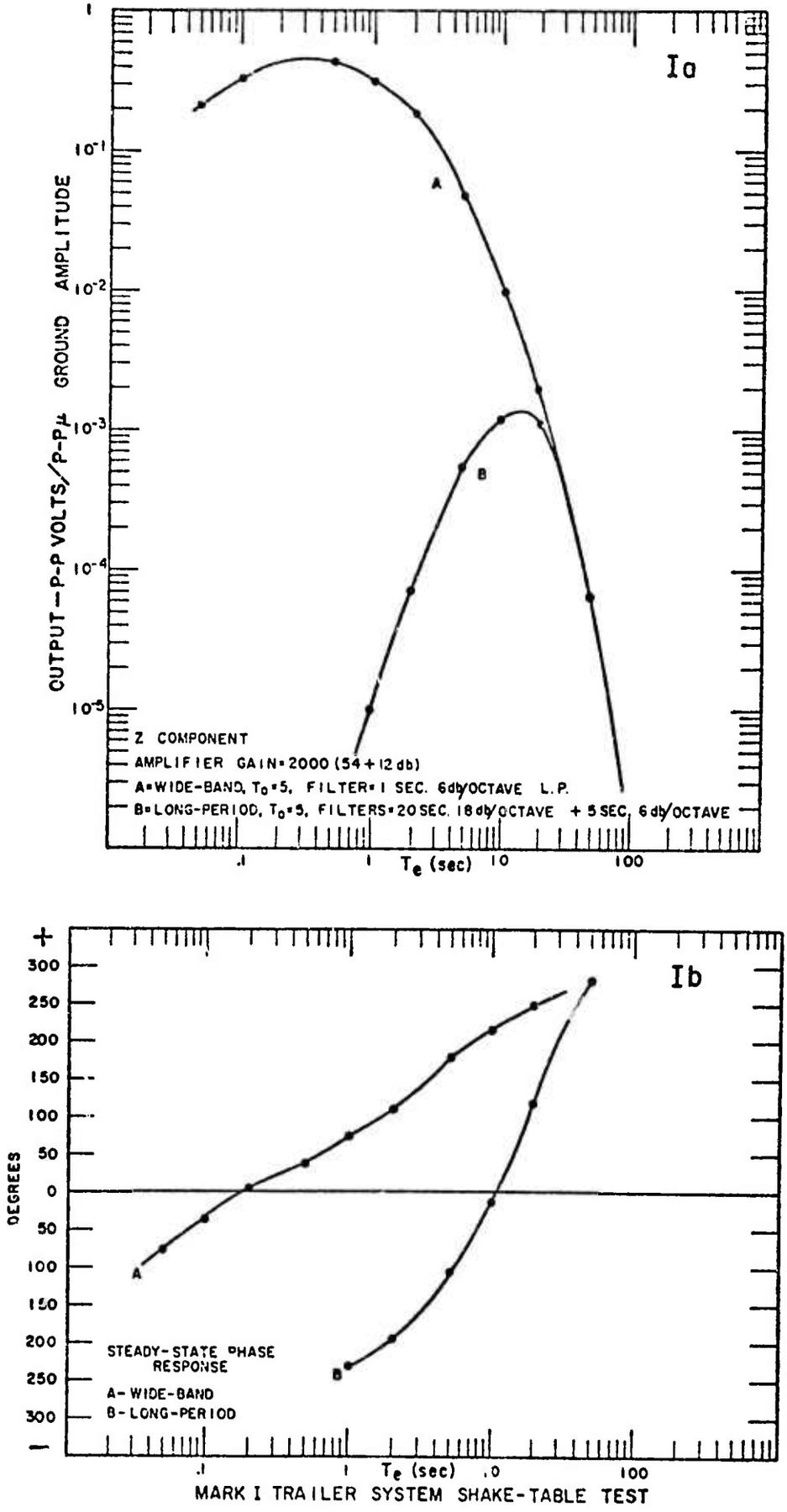
Ia
CUTPUT — P-P VOLTS/P-P μ GROUND AMPLITUDE
1
10⁻¹
10⁻²
10⁻³
10⁻⁴
10⁻⁵
A
B
Z COMPONENT
AMPLIFIER GAIN=2000 (54+12 db)
A=WIDE-BAND, T₀=5, FILTER=1 SEC. 6db/OCTAVE L.P.
B=LONG-PERIOD, T₀=5, FILTERS=20 SEC. 18 db/OCTAVE + 5 SEC. 6 db/OCTAVE
.1
1
Tₑ (sec)
10
100
Ib
+
300
250
200
150
100
50
0
50
100
150
200
250
300
—
DEGREES
A
B
STEADY-STATE PHASE RESPONSE
A- WIDE-BAND
B- LONG-PERIOD
.1
1
Tₑ (sec)
.0
100
MARK I TRAILER SYSTEM SHAKE-TABLE TEST

Figure 2

Mark I units may, however, be left in the field to provide additional coverage of the monitored site provided we can afford the costs.)

The system response of the Mark I and II portable trailer units have been obtained by shake-table tests and are given in Figures 1 through 4. Figure 1 shows the pass band and gains available from the amplifiers used in these systems. Figure 2 gives the amplitude and phase response for the Mark I systems operating either as broadband recorders or as "long period" recording systems. To date we have found that the Mark I systems function exceptionally well as long period recording systems. In the next section (II-2) we show two small earthquakes (m_b = 4 and m_b = 3.5) from the Bear Valley area as examples of this recording capability.

Figure 3 shows the system response of the Mark II units with third order low pass filtering at the various filter settings available. Curve C, with the filter setting at 20 sec is equivalent to Curve B in Figure 2 which shows the long period response of the Mark I units. This response is what we are currently using in the field.

Figure 4 shows the response of two Mark II systems using fourth order low-pass filtering and the available variety of pass bands. Either the third or fourth order filters can be used.

(2) Station Configuration and Events Recorded

Figure 5 shows the configuration of the Bear Valley array along with a general identification of instruments employed and field program participants. This array has been completely operational for only the last 4-5 months and in that period no events occurred within the central monitored area, nor in fact within the general area enclosed by the most

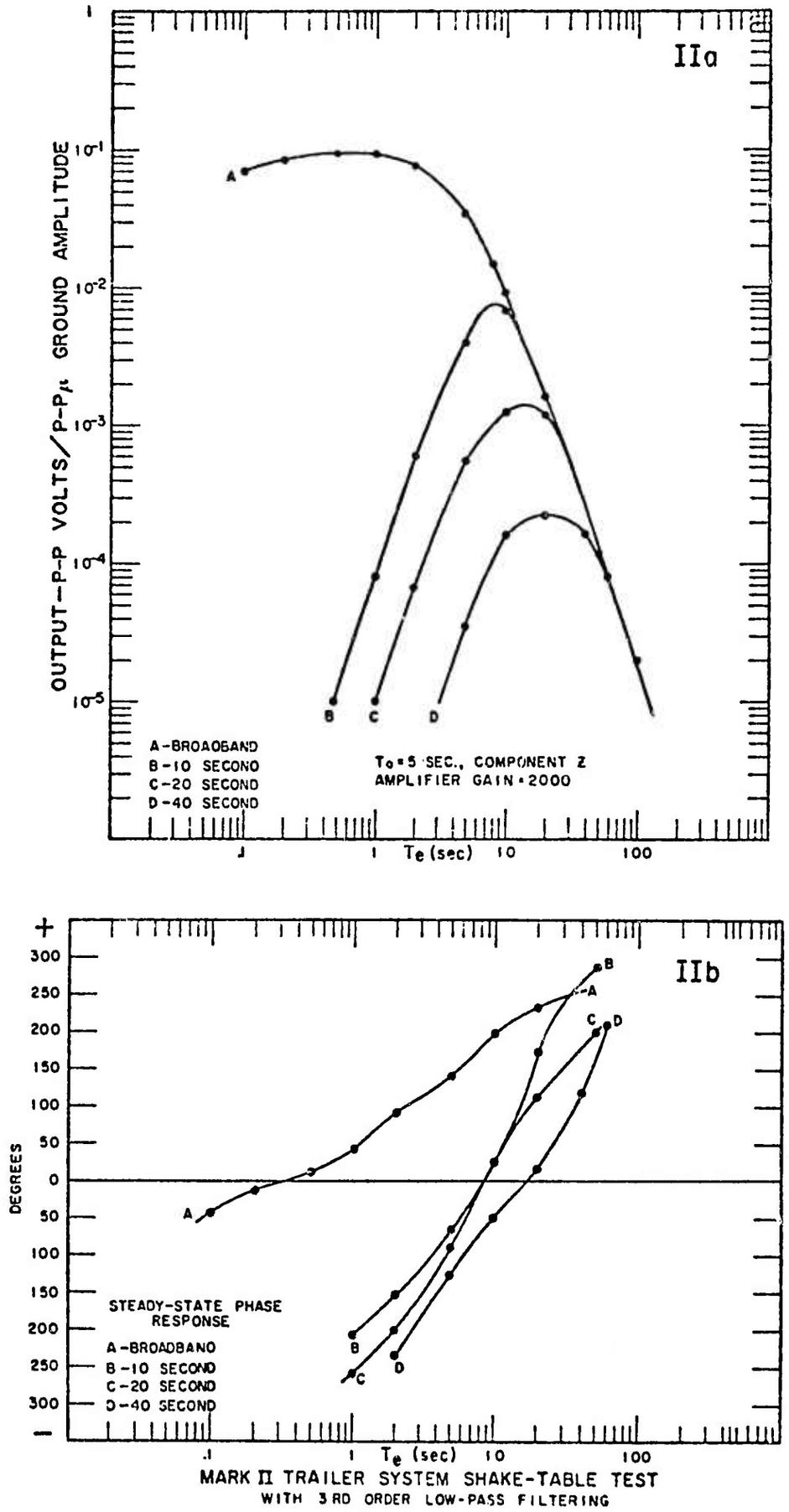
IIa
OUTPUT—P-P VOLTS/P-P$_\mu$ GROUND AMPLITUDE
10^{-1}
10^{-2}
10^{-3}
10^{-4}
10^{-5}
A
B
C
D
A-BROADBAND
B-10 SECOND
C-20 SECOND
D-40 SECOND
T_o=5 SEC., COMPONENT Z
AMPLIFIER GAIN=2000
.1
1
T_e (sec)
10
100
IIb
+
300
250
200
150
100
50
0
50
100
150
200
250
300
−
DEGREES
STEADY-STATE PHASE RESPONSE
A-BROADBAND
B-10 SECOND
C-20 SECOND
D-40 SECOND
.1
1
T_e (sec)
10
100
MARK II TRAILER SYSTEM SHAKE-TABLE TEST
WITH 3RD ORDER LOW-PASS FILTERING

Figure 3

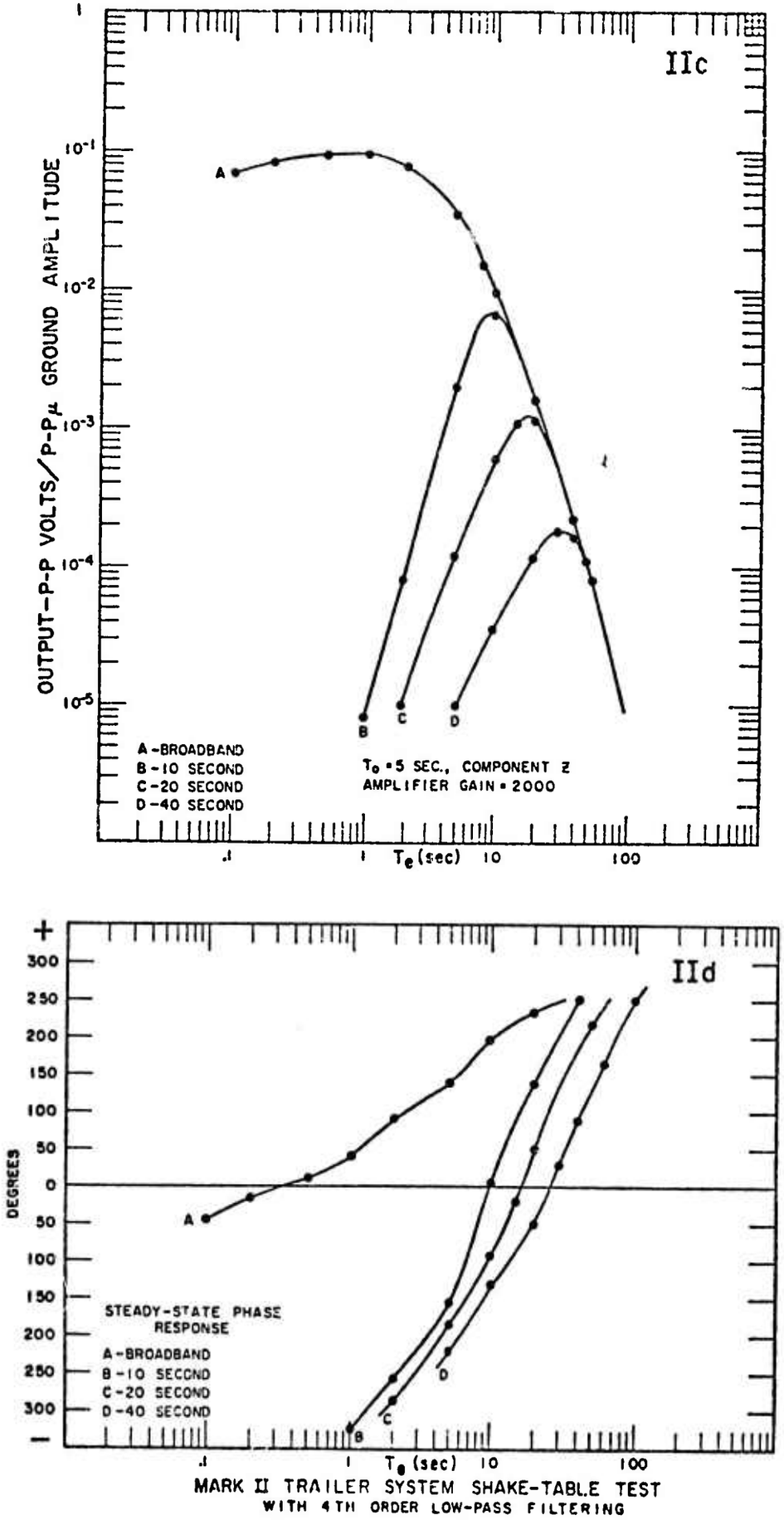

MARK II TRAILER SYSTEM SHAKE-TABLE TEST
WITH 4TH ORDER LOW-PASS FILTERING

Figure 4

extremely separated elements of the array. However, prior to the completion of the array two small events occurred which were recorded by our long period trailers. Even though we cannot analyze these events using the full array, the recordings provide a demonstration of the ability of these portable units to adequately record long period radiation from events in the magnitude range of interest. Figure 6 shows the two events as recorded by one of the trailer units.

It is felt that the units presently in the field will record m_b = 3.5 events out to the most extreme distance and that the Mark II units will be somewhat more sensitive.

III. Theoretical Developments

In anticipation of successfully recording earthquakes in the near and far field distance ranges during this program we have developed the theoretical framework for the interpretation of near and far field wave propagation effects as well as a more comprehensive relaxation source representation which treats near field effects in detail.

The problems faced in treating the near field of an earthquake are two-fold. First: An earthquake is a volume source, in that energy is released from within some finite volume resulting in a net decrease in stored strain energy within that region; the question then is whether measurements of the radiation field made within this source volume will be fundamentally different than measurements made when outside of it. In the near field it is quite literally the case that the real source is distributed in space all around the point of observation instead of being localized at some point, or on some surface. In this case, the usual

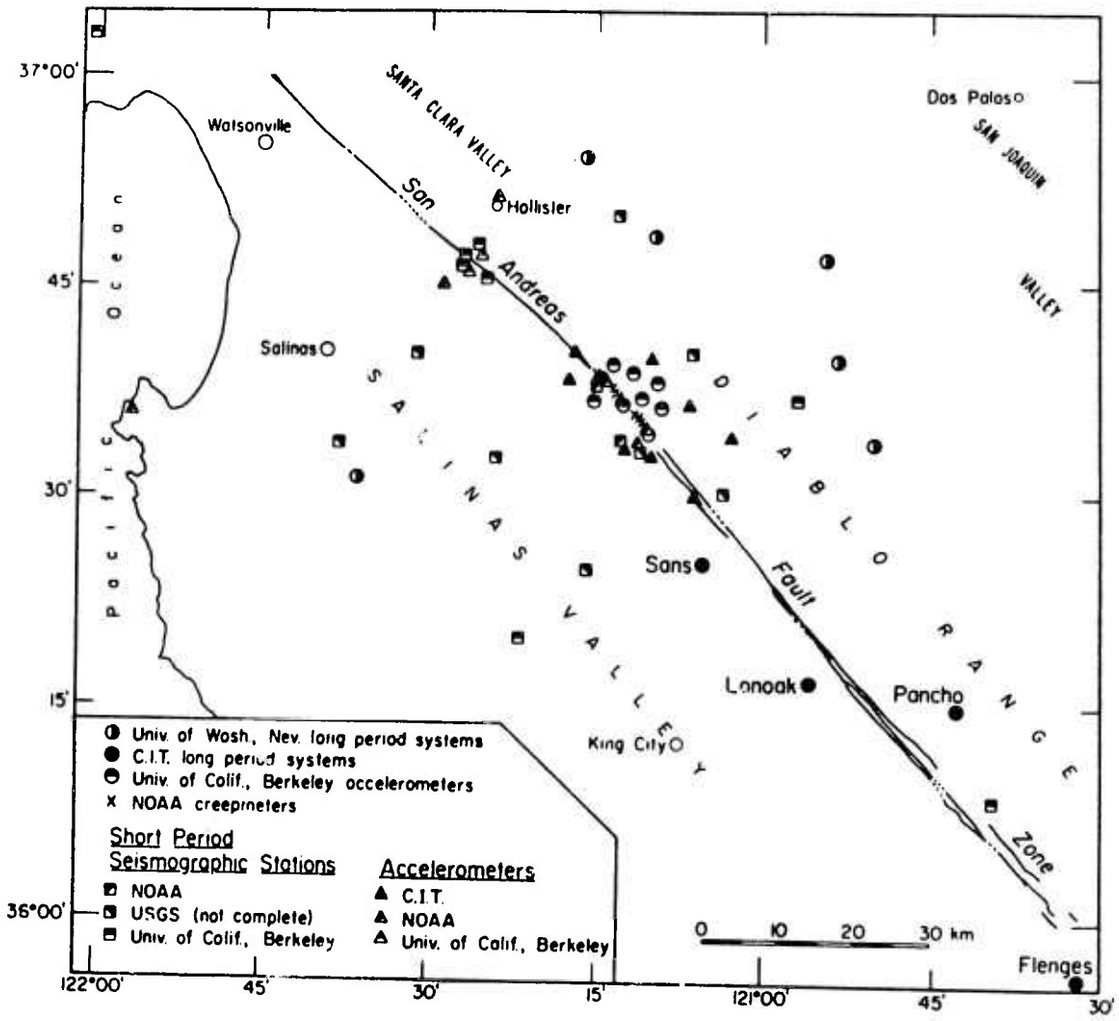
37°00'
45'
30'
15'
36°00'
122°00'
45'
30'
15'
121°00'
45'
30'
Watsonville
Hollister
Salinas
Sans
Lonoak
Pancho
King City
Flenges
Dos Palos
SANTA CLARA VALLEY
San Andreas Fault Zone
SAN JOAQUIN VALLEY
SALINAS VALLEY
DIABLO RANGE
Pacific Ocean
Univ. of Wash., Nev. long period systems
C.I.T. long period systems
Univ. of Calif., Berkeley accelerometers
NOAA creepmeters
Short Period Seismographic Stations
NOAA
USGS (not complete)
Univ. of Calif., Berkeley
Accelerometers
C.I.T.
NOAA
Univ. of Calif., Berkeley
0 10 20 30 km

Figure 5

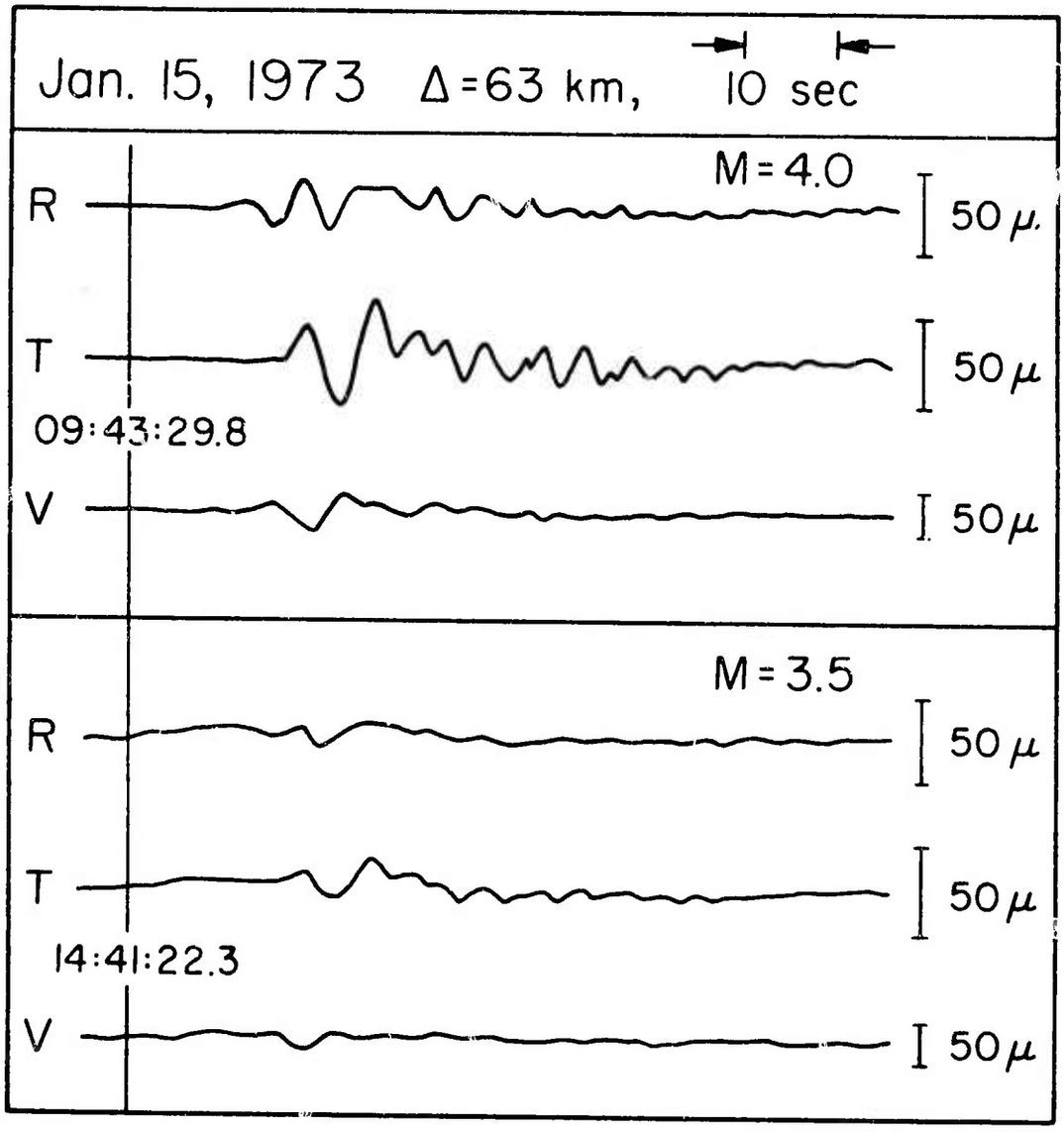
Jan. 15, 1973 Δ=63 km,
10 sec
M=4.0
R
T
V
50 μ
50 μ
50 μ
09:43:29.8
M=3.5
R
T
V
50 μ
50 μ
50 μ
14:41:22.3

Figure 6

theoretical treatments of energy radiation, which assume a localized source, are inadequate, or at least have implicit in their formulation an assumption regarding the spatial origins of the energy release which are extremely restrictive.

Thus the problem is to determine the field to be observed at a point which is within the source itself; in the case of an earthquake, within the zone of stress relaxation.

The second problem is that conventional "far field" approximations used in wave propagation theory must be given up and the propagation of energy in the rather complex medium must be calculated more exactly for near field observations. Furthermore, interference effects related to multiple reflections, and hence waveguide phenomena giving rise to ordinary surface waves, for example, cannot be fully effective in the near source region since the required constructive or destructive interaction of reflected, refracted and diffracted waves will not have completely occurred. This means that, in the very near source region, it is necessary to calculate the field using a Cagniard (or generalized ray theory) method which takes explicit account of individual generalized rays and sums them to provide the predicted radiation field. Alternatively, the so-called "leaking mode" theory can be used, or a full numerical calculation using finite difference or finite element methods.

In addressing ourselves to these problems, we decided in the first place that the problems were such that without special attention devoted to them, one could not hope to obtain a meaningful interpretation of the field data to be obtained in this program. Therefore we began investigations in three separate areas; (1) on the theory of the source in the near field range for the receiver inside the prestress zone as well as outside the zone;

(2) on the inclusion of complex relaxation source models in surface wave propagation programs wherein all near field effects are included; (3) and on the inclusion of complex source models in the Cagnaird genralized ray theory, again retaining the near distance radiation effects from the source. Further, in conjunction with other work related to earthquake-explosion discrimination, we began systematic investigations of source characteristics utilizing these theoretical capabilities.

In the following subsections (II-1 through II-3) we summarize, in some detail, the results of the theoretical investigations. In Section IV we give a summary of some of the preliminary results obtained through applications of the theory to the discrimination problem, particularly in terms of source characteristics which lead to discrimination on the basis of m_b vs M_S.

(1) Extensions of Relaxation Source Theory for Near Field Representations

The solution can be expressed in terms of potentials. Archambeau (1972) obtained (eq. 5-1).

$$\chi_\alpha^{(1)}(\underline{r},t) = -\frac{1}{4\pi V_\alpha^2}\int_0^{\tau_o} dt_o \iiint_{V(t_o)} \frac{\partial \chi_\alpha^*}{\partial t_o}\left(\frac{\delta_1\left(\frac{r^*}{V_\alpha} - t + t_o\right)}{r^*}\right)\underline{dr}_o \qquad (1)$$

χ_α $\alpha = 1...4$ represent the three components of rotation and the dilatation. V_α is the appropriate wave velocity, χ_α^* are the equilibrium fields appropriate to a moving boundary Σ in the medium. $V(t_o)$ is the volume exterior to Σ, as a function of t_o, the source time, and τ_o is the total rupture time.

For the case of the self similar problem, where Σ is an expanding spherical rupture, $V(t_o)$ is the volume exterior to that sphere.

However for the case of a propagating spherical rupture, we will use an approximation, necessitated by the lack of symmetry of the problem. In particular, we shall consider the case of a unilateral rupture and consider a spherical rupture propagating from the point 0' along the $X_3^{(0)}$ axis, with a radius $R(t_o)$, and center at $d(t_o)$ on this axis (Figure 1). Because of theoretical complications associated with healing phenomena (after rupture), the treatment given in this report will be confined to the case

$$d(t_o) \leq R(t_o)$$

More complicated rupture geometries, of greater generality, will be treated later. However, this "enveloping" model will show all the essential characteristics of importance.

In order to preserve the symmetry of the problem, the volume of integration $V(t_o)$ is then defined as the volume exterior to the sphere $B(t_o)$ (Figure 1), centered at the hypocenter, and going through the rupture front. The radius of this sphere is then $V_R t_o$. This neglects contributions from inside $B(t_o)$ but the approximation is justified by the fact that all of the non-elastic phenomena associated with failure take place within $B(t_o)$, and the elastic energy stored inside $B(t_o)$ can safely be assumed to be dissipated by these phenomena.

It is convenient to take Fourier transforms of (1) with respect to t, and then we have

$$\tilde{\chi}_\alpha(\underline{r},\omega) = \frac{i\omega}{4\pi V_\alpha^2} \int_0^{\tau_o} e^{-i\omega t_o} \int_{V(t_o)} \frac{\partial \chi_\alpha^*}{\partial t_o} \frac{e^{-ik_\alpha r^*}}{r^*} \underline{dr}_o \, dt_o \qquad (2)$$

The function $e^{-ik_\alpha r^*}/r^*$ is the Green's function for the Helmholtz equation in the infinite domain. Its use in equation (2) is an approximation: The solution given by (2) will satisfy the initial value conditions, but $\chi_\alpha(r,t)$ will not necessarily satisfy the appropriate boundary conditions on Σ for all t. In order to satisfy those boundary conditions, one would have to superpose general solutions of the homogeneous equations and (2). This additional term would in essence represent the interaction of the dynamic fields with the boundary Σ, in other words, the scattered fields. Ignoring

the scattered fields is equivalent to making the inclusion within Σ transparent to incoming waves and can indeed be taken as the definition of transparency. To model underground explosions, we consider an expanding sphere of radius $R(t_o)$, upon which the tractions vanish, center at 0'. The initial values χ_α^* are given by

$$\chi_\alpha^*(\underline{r}_o, t_o) = \frac{1}{(r_o)^3} \sum_{m=0}^{2} \left(a_{2m}^{(\alpha)} \cos m\,\phi_o + b_{2m}^{(\alpha)} \sin m\,\phi_o \right) P_2^m (\cos\theta_o) \tag{3}$$

Where the coefficients $a_{2m}^{(\alpha)}$ and $b_{2m}^{(\alpha)}$ are given by Archambeau (1972, eq. 4.9 and 4.10)

$$a_{2m}^{(\alpha)}(t) = \frac{5\left[(1-\sigma)-\delta_{\alpha 4}\sigma\right]}{\mu(7-5\sigma)} R^3(t_o) \begin{pmatrix} -3\sigma_{23}^{(0)}/2 & -\sigma_{12}^{(0)}/2 & -\sigma_{23}^{(0)}/4 \\ 3\sigma_{13}^{(0)}/2 & 0 & \sigma_{13}^{(0)}/4 \\ 0 & \sigma_{23}^{(0)}/2 & \sigma_{12}^{(0)}/2 \\ 0 & \sigma_{13}^{(0)} & 0 \end{pmatrix} \tag{4.1}$$

$$= a'^{(\alpha)}_{2m} \cdot R^3(t_o)$$

$$b_{2m}^{(\alpha)}(t_o) = \frac{5\left[(1-\sigma)-\delta_{\alpha 4}\sigma\right]}{\mu(7-5\sigma)} R^3(t_o) \begin{pmatrix} 0 & 0 & \sigma_{13}^{(0)}/4 \\ 0 & \sigma_{12}^{(0)}/2 & -\sigma_{23}^{(0)}/4 \\ 0 & -\sigma_{13}^{(0)}/2 & 0 \\ 0 & \sigma_{23}^{(0)} & \sigma_{12}^{(0)}/2 \end{pmatrix} \tag{4.2}$$

$$= b'^{(\alpha)}_{2m} \cdot R^3(t_o)$$

where $\sigma_{ij}^{(0)}$ represents the prestress, chosen to be pure shear and homogeneous for this case.

On the other hand, in the case of a propagating rupture, one has to take into account the fact that at time t_o, the failure zone is centered on the X_3' axis at a distance $d(t_o)$ from O'. Using addition theorems for the Legendre associated functions one gets in that case

$$\chi_\alpha^*(\underline{r}_o, t_o) = \frac{1}{r_o^3} \sum_{m=0}^{2} \left(a_{2m}^{(\alpha)} \cos m \phi_o + b_{2m}^{(\alpha)} \sin m \phi_o \right) \cdot \sum_{s=0}^{\infty} \frac{(2-m+s)!}{s!(2-m)!} \left[\frac{d(t_o)}{r_o} \right]^s P_{2+s}^m (\cos \theta_o) \tag{5}$$

where the coefficients $a_{2m}^{(\alpha)}(t_o)$ and $b_{2m}^{(\alpha)}(t_o)$ are again given by (4.1) and (4.2). Note that only the harmonics of degree 2 are present. This is not the case for non-spherical ruptures.

Therefore we see that (3) is merely a particular case of (5) where the sum over the index s is reduced to its first term s = 0. (5) is only valid for $r_o < d(t_o)$, however, this is always the case for $\underline{r}_o \in V(t_o)$.

The initial value $\chi_\alpha^*(\underline{r}_o, t_o)$ vanishes like $\frac{1}{r_o^3}$ at $r_o \to \infty$. However, if only because of the finiteness of the earth, and because the present $\sigma_{ij}^{(0)}$ can hardly be homogeneous at very large distances from the source, one may assume that this initial value becomes vanishingly small beyond a relaxation radius R_S. The simplest way to approximate such a behavior

is to use the initial value given by (3) or (5) in (2), but to truncate the volume integral in (2) at the radius R_S. The volume within R_S will be henceforth referred to as the relaxation zone. Two possible geometries then arise. In a first instance, the relaxation zone may be confined to the vicinity of the failure, so that most observer's points $\underline{r}$ would lie outside of it. This is the geometry investigated previously by Archambeau (1968). Archambeau showed that the error on the energy released is negligible provided that R_S is equal to about five times the fault length d_o. This case we shall consider as one possible extreme behavior - the other geometry corresponds to the case where R_S may be large and, in the limit, infinite - observer points then lie within the relaxation zone. This constitutes another extreme behavior.

These two extreme behaviors will allow us to place bounds on the spectral content of the radiation fields, the reality being, of course, between these extremes.

We shall now treat the case of a propagating rupture, with a finite relaxation zone and an observer inside this relaxation zone. This is the most general case, and the results appropriate to the extreme geometries, as well as the results for non-propagating ruptures may be deduced easily thereafter.

We first rewrite equation (2) in the form:

$$\tilde{\chi}_\alpha(r,\omega) = \frac{i\omega}{4\pi V_\alpha^2} \int_0^{2\pi} d\phi_o \int_0^{\pi} \sin\theta_o \, d\theta_o \cdot \int_0^{\tau_o} dt_o \int_{V_R t_o}^{R_s} \frac{\partial \chi_\alpha^*}{\partial t_o} \frac{e^{-ik_\alpha r^*}}{r^*} r_o^2 dr_o \qquad (6)$$

Equation (6) is obviously valid for any of the cases considered above. We shall make use of the usual spherical wave expansions

$$\frac{e^{ik_\alpha r^*}}{r^*} = -ik_\alpha \sum_{\ell=0}^{\infty} (2\ell+1)\, P_\ell(\cos\gamma) \begin{pmatrix} j_\ell(k_\alpha r_o)\, h_\ell^{(2)}(k_\alpha r) \\ j_\ell(k_\alpha r)\, h_\ell^{(2)}(k_\alpha r_o) \end{pmatrix} \qquad (7)$$

where the upper pair of Bessel functions are to be used when $|\underline{r}| > |\underline{r}_o|$, and the lower pair when $|\underline{r}_o| > |\underline{r}| > d_o$.

Here

$$P_\ell(\cos\gamma) = \sum_{k=0}^{\ell} (2-\delta_{ko}) \frac{(\ell-k)!}{(\ell+k)!} P_\ell^k(\cos\theta)\, P_\ell^k(\cos\theta_o) \cdot \cos k(\phi-\phi_o) \qquad (8)$$

where δ_{ko} is the usual Kronecker delta. We shall also use the integral relation

$$\int_0^{2\pi}\int_0^{\pi} P_\ell(\cos\gamma)\, P_\nu^\mu(\cos\theta_o)\begin{pmatrix}\cos\mu\phi_o\\ \sin\mu\phi_o\end{pmatrix}\sin\theta_o\, d\theta_o\, d\phi_o =$$

$$\frac{4\pi}{2\ell+1}\, P_\ell^\mu(\cos\theta)\begin{pmatrix}\cos\mu\,\phi_o\\ \sin\mu\,\phi_o\end{pmatrix}\,\delta_{\ell\nu} \tag{9}$$

Using (7), (8), (9) in (6), inserting (5) for χ_α^* where appropriate, and splitting the last integral in (6) as

$$\int_{V_R t_o}^{R_s} = \int_{V_R t_o}^{r} + \int_r^{R_s}$$

gives

$$\tilde{\chi}_\alpha(\underline{r},\omega) = \sum_{\ell=2}^{\infty}\sum_{m=0}^{2} P_\ell^m(\cos\theta)$$

$$\cdot\left[h_\ell^{(2)}(k_\alpha r)\left({}_\ell A_{2m}^{(\alpha)}\cos m\phi + {}_\ell B_{2m}^{(\alpha)}\sin m\phi\right)\right. \tag{10}$$

$$\left. + j_\ell(k_\alpha r)\left({}_\ell C_{2m}^{(\alpha)}\cos m\phi + {}_\ell D_{2m}^{(\alpha)}\sin m\phi\right)\right]$$

where the multipole coefficients ${}_\ell A_{2m}$, ${}_\ell B_{2m}$, ${}_\ell C_{2m}$, ${}_\ell D_{2m}$, are given by:

$$\begin{pmatrix} {}_{\ell}A_{2m}^{(\alpha)}(r,\omega) \\ {}_{\ell}B_{2m}^{(\alpha)}(r,\omega) \end{pmatrix} = \begin{pmatrix} a'^{(\alpha)}_{2m} \\ b'^{(\alpha)}_{2m} \end{pmatrix} \frac{(\ell-m)!}{(\ell-2)!\ (2-m)!} \frac{k_\alpha^2}{V_\alpha}$$

$$\cdot \int_0^{\tau_o} e^{-i\omega t_o} \frac{\partial}{\partial t_o} \left[R^3(t_o)\ d^{\ell-2}(t_o) \right] \int_{V_R t_o}^{r} \left(\frac{1}{r_o}\right)^{\ell+1} j_\ell(k_\alpha r_o) r_o^2\ dr_o\ dt_o \tag{11}$$

$$\begin{pmatrix} {}_{\ell}C_{2m}^{(\alpha)}(r,\omega) \\ {}_{\ell}D_{2m}^{(\alpha)}(r,\omega) \end{pmatrix} = \begin{pmatrix} a'^{(\alpha)}_{2m} \\ b'^{(\alpha)}_{2m} \end{pmatrix} \frac{(\ell-m)!}{(\ell-2)!\ (2-m)!} \frac{k_\alpha^2}{V_\alpha}$$

$$\cdot \int_0^{\tau_o} e^{-i\omega t_o} \frac{\partial}{\partial t_o} \left[R^3(t_o)\ d^{\ell-2}(t_o) \right] \int_{r}^{R_s} \left(\frac{1}{r_o}\right)^{\ell+1} h_\ell^{(2)}(k_\alpha r_o) r_o^2\ dr_o\ dt_o \tag{12}$$

For the non-propagating rupture, because symmetry is preserved, only the term $\ell = 2$ survives in (10), (11) and (12).

Despite its symmetry, solution (10) is not particularly convenient since the multipole coefficients depend on r, the hypocentral distance of the observer. A more convenient form for computation can be obtained by evaluating the integrals in (11) and (12).

It can be shown (Minster, 1973) that

$$\int_a^b (r_o)^{-(\ell+1)}\, j_\ell(k_\alpha r_o)\, r_o^2 dr_o = \frac{j_{\ell-1}(k_\alpha a)}{k_\alpha\, a^{\ell-1}} - \frac{j_{\ell-1}(k_\alpha b)}{k_\alpha\, b^{\ell-1}}$$

$$\int_a^b (r_o)^{-(\ell+1)}\, h_\ell^{(2)}(k_\alpha r_o)\, r_o^2\, dr_o = \frac{h_{\ell-1}^{(2)}(k_\alpha a)}{k_\alpha\, a^{\ell-1}} - \frac{h_{\ell-1}^{(2)}(k_\alpha b)}{k_\alpha\, b^{\ell-1}}$$

Inserting these formulae into (11) and (12) one gets

$$\begin{pmatrix} {}_\ell A_{2m}^{(\alpha)}(r,\omega) \\ {}_\ell B_{2m}^{(\alpha)}(r,\omega) \end{pmatrix} = \begin{pmatrix} a_{2m}'^{(\alpha)} \\ b_{2m}'^{(\alpha)} \end{pmatrix} \frac{(\ell-m)!}{(\ell-2)!\,(2-m)!} \frac{k_\alpha^\ell}{V_\alpha}$$

$$\cdot \int_0^{\tau_o} e^{-i\omega t_o} \frac{\partial}{\partial t_o}\left[R^3(t_o)\, d^{\ell-2}(t_o)\right]\left[\frac{j_{\ell-1}(k_\alpha V_R t_o)}{(k_\alpha V_R t_o)^{\ell-1}} - \frac{j_{\ell-1}(k_\alpha r)}{(k_\alpha r)^{\ell-1}}\right] dt_o \qquad (13)$$

and

$$\begin{pmatrix} {}_\ell C_{2m}^{(\alpha)}(r,\omega) \\ {}_\ell D_{2m}^{(\alpha)}(r,\omega) \end{pmatrix} = \begin{pmatrix} a_{2m}'^{(\alpha)} \\ b_{2m}'^{(\alpha)} \end{pmatrix} \frac{(\ell-m)!}{(\ell-2)!\,(2-m)!} \frac{k_\alpha^\ell}{V_\alpha}$$

$$\cdot \int_0^{\tau_o} e^{-i\omega t_o} \frac{\partial}{\partial t_o}\left[R^3(t_o)\, d^{\ell-2}(t_o)\right]\left[\frac{h_{\ell-1}^{(2)}(k_\alpha r)}{(k_\alpha r)^{\ell-1}} - \frac{h_{\ell-1}^{(2)}(k_\alpha R_s)}{(k_\alpha R_s)^{\ell-1}}\right] dt_o \qquad (14)$$

One sees immediately that the only integrals left to evaluate are

$$I_\ell^{(1)}(\omega) = \int_0^{\tau_o} e^{-i\omega t_o} \frac{d}{dt_o}\left[R^3(t_o)\, d^{\ell-2}(t_o)\right] dt_o$$

which can be evaluated in closed form (Minster and Archambeau, 1973) and

$$I_\ell^{(2)}(\omega) = \int_0^{\tau_o} e^{-i\omega t_o} \frac{d}{dt_o}\left[R^3(t_o)\, d^{\ell-2}(t_o)\right] \frac{j_{\ell-1}(k_\alpha V_R t_o)}{\left(k_\alpha V_R t_o\right)^{\ell-1}}\, dt_o \,,$$

for which closed forms can be found, but which is nevertheless best computed numerically as a finite Fourier transform.

We can now combine the r dependent terms in (13) and (14), and make use in (10) of the Wronskian relation

$$j_\ell(kr)\, h_{\ell-1}^{(2)}(kr) - h_\ell^{(2)}(kr)\, j_{\ell-1}(kr) = -\frac{i}{k^2 r^2}$$

This allows us to write the solution in the final form.

$$\tilde{\chi}_\alpha(\underline{r},\omega) = \sum_{\ell=2}^{\infty} \sum_{m=0}^{2} P_\ell^m(\cos\theta)\left[h_\ell^{(2)}(k_\alpha r)\left(A_{\ell m}^{(\alpha)} \cos m\phi + B_{\ell m}^{(\alpha)} \sin m\phi\right)\right.$$

$$+ \frac{i}{(k_\alpha r)^{\ell+1}}\left(C_{\ell m}^{(\alpha)} \cos m\phi + D_{\ell m}^{(\alpha)} \sin m\phi\right)$$

$$\left. + j_\ell(k_\alpha r)\left(E_{\ell m}^{(\alpha)} \cos m\phi + F_{\ell m}^{(\alpha)} \sin m\phi\right)\right] \qquad (15)$$

where

$$\begin{pmatrix} A_{\ell m}^{(\alpha)}(\omega) \\ B_{\ell m}^{(\alpha)}(\omega) \end{pmatrix} = \begin{pmatrix} a'_{2m} \\ b'_{2m} \end{pmatrix} \frac{(\ell-m)!}{(\ell-2)!\ (2-m)!} \frac{k_\alpha^\ell}{V_\alpha} I_\ell^{(2)}(\omega)$$

$$\begin{pmatrix} C_{\ell m}^{(\alpha)}(\omega) \\ D_{\ell m}^{(\alpha)}(\omega) \end{pmatrix} = -\begin{pmatrix} a'_{2m} \\ b'_{2m} \end{pmatrix} \frac{(\ell-m)!}{(\ell-2)!\ (2-m)!} \frac{k_\alpha^\ell}{V_\alpha} I_\ell^{(1)}(\omega)$$

$$\begin{pmatrix} E_{\ell m}^{(\alpha)}(\omega) \\ F_{\ell m}^{(\alpha)}(\omega) \end{pmatrix} = + \frac{h_{\ell-1}^{(2)}(k_\alpha R_s)}{(k_\alpha R_s)^{\ell-1}} \begin{pmatrix} C_{\ell m}^{(\alpha)}(\omega) \\ D_{\ell m}^{(\alpha)}(\omega) \end{pmatrix} \tag{16}$$

The analysis proceeds in an identical fashion for the non-propagating case, by keeping only the $\ell = 2$ term. The second term in equation (15) is a non propagating term; in fact, it represents the creation of the initial value. To see this take the Fourier transform of (5)

$$\tilde{\chi}_\alpha^*(\underline{r},\omega) = \sum_{s=0}^{\infty} \sum_{m=0}^{2} \frac{(2-m+s)!}{s!(2-m)!} \frac{1}{r^{s+3}} \left(\tilde{a}_{2m}^{(\alpha)}(\omega) \cos m\phi + \tilde{b}_{2m}^{(\alpha)} \sin m\phi \right)$$

$$\cdot P_{s+2}^m(\cos\theta)$$

which by simple redefinition of the indices can be rewritten

$$\tilde{\chi}^{*}_{\alpha}(\underline{r},\omega) = \sum_{\ell=2}^{\infty} \sum_{m=0}^{2} P_{\ell}^{m}(\cos\theta) \left(\frac{+i}{(k_{\alpha}r)^{\ell+1}} \right) \left(C_{\ell m}^{(\alpha)} \cos m\phi + D_{\ell m}^{(\alpha)} \sin m\phi \right) \qquad (17)$$

because (15.) gives us the relative field, (measured with respect to the final equilibrium), one has to subtract (17) from (15) to obtain the observed radiation field.

We are now in a position to investigate the extreme cases presented above.

1) If we take R_s infinite, then we have immediately

$$\tilde{\chi}_{\alpha}(\underline{r},\omega) = \sum_{\ell=2}^{\infty} \sum_{m=0}^{2} h_{\ell}^{(2)}(k_{\alpha}r) \left(A_{\ell m}^{(\alpha)}(\omega) \cos m\phi + B_{\ell m}^{(\alpha)}(\omega) \sin m\phi \right) \cdot P_{\ell}^{m}(\cos\theta) \qquad (18)$$

2) In the case of a limited relaxation zone $R_S < r$ we need only keep the first term in (10) and change the upper limit of the integral over r_o in (11) to R_S - consequently the solution has the same form as (18) and the integral $I_{\ell}^{(2)}(\omega)$ appearing in (16) has to be replaced by

$$I_{\ell}^{(3)}(\omega) = \int_{0}^{\tau_o} e^{-i\omega t_o} \frac{d}{dt_o} \left[R^3(t_o)\, d^{\ell-2}(t_o) \right] \left[\frac{j_{\ell-1}(k_{\alpha}V_R t_o)}{(k_{\alpha}V_R t_o)^{\ell-1}} - \frac{j_{\ell-1}(k_{\alpha}R_s)}{(k_{\alpha}R_S)^{\ell-1}} \right] dt_o$$

This is specifically the case investigated by Archambeau (1968).

Long period behavior of the spectra

Let us first investigate the long period behavior of $I_\ell^{(2)}(\omega)$ and $I_\ell^{(3)}(\omega)$. It is easy to show that

$$I_\ell^{(2)}(\omega) = \frac{1}{1.3....(2\ell-1)} \cdot R^3(\tau_o)\, d^{\ell-2}(\tau_o) + 0(\omega) \text{ for } \omega << 1$$

$$I_\ell^{(3)}(\omega) = \frac{1/2 \quad k_\alpha^2}{1.3....(2\ell+1)} \int_0^{\tau_o} \frac{d}{dt_o} \left(R^3(t_o)\, d^{\ell-2}(t_o) \right) \left[R_S^2 - (V_R t_o)^2 \right] dt_o$$

$$+ 0(\omega^3) \text{ for } \omega << 1$$

therefore the following results hold

1) $\underline{R_s < r}$

$$\begin{pmatrix} A_m^{(\alpha)} \\ B_m^{(\alpha)} \end{pmatrix} = \begin{pmatrix} a'_{2m} \\ b'_{2m} \end{pmatrix} \frac{(\ell-m)!}{(\ell-2)!\ (2-m)!} \frac{1/2}{1.3....(2\ell+1)} \frac{k_\alpha^{\ell+2}}{V_\alpha}$$

$$\cdot \int_0^{\tau_o} \frac{d}{dt_o} \left(R^3(t_o)\, d^{\ell-2}(t_o) \right) \left[R_S^2 - (V_R t_o)^2 \right] dt_o + 0(\omega^{\ell+3})$$

for $\omega << 1$

(19)

2) $\underline{R_S = \infty}$

$$\begin{pmatrix} A_{\ell m}^{(\alpha)} \\ B_{\ell m}^{(\alpha)} \end{pmatrix} = \begin{pmatrix} a'_{2m} \\ b'_{2m} \end{pmatrix} \frac{(\ell-m)!}{(\ell-2!\ (2-m)!} \frac{R^3(\tau_o)\ d^{\ell-2}(\tau_o)}{1.3....(2\ell-1)} \frac{k_\alpha^\ell}{V_\alpha} + 0(\omega^{\ell+1}) \text{ for } \omega << 1 \tag{20}$$

furthermore we can write

$$h_\ell^{(2)}(k_\alpha r) = i^{\ell+1} \frac{e^{-ik_\alpha r}}{k_\alpha r} \sum_0^\ell (\ell+ 1/2,\ k)\ (2ik_\alpha r)^{-k}$$

where

$$(\ell + 1/2, k) = \frac{(\ell+k)!}{k!\Gamma(\ell-k+1)}$$

I. <u>Farfield approximation</u> $k_\alpha r << 1$

In this case we approximate the Hankel function by its far field term

$$h_\ell^{(2)}(k_\alpha r) \sim i^{\ell+1} \frac{e^{-ik_\alpha r}}{k_\alpha r}$$

The spectral shape is then easily obtained, because only the quadrupole term is important for long periods.

1) $R_S \ll r$

$$\left.\begin{aligned} \left[\tilde{\chi}_\alpha(\omega)\right]_F &= 0(\omega^3) \\ \left[\tilde{u}(\omega)\right]_F &= 0(\omega^2) \end{aligned}\right\} \quad \text{for } \omega \ll 1$$

This result is the one obtained by Archambeau in previous studies. It implies that the displacement spectrum exhibits at least one peak. The displacement spectral density vanishes as ω^2 at long period.

2) $R_S = \infty$

$$\text{Then} \left.\begin{aligned} \left[\tilde{\chi}_\alpha(\omega)\right]_F &= 0(\omega) \\ \left[\tilde{u}(\omega)\right]_F &= 0(1) \end{aligned}\right\} \quad \text{for } \omega \ll 1$$

This gives a spectral shape similar to that suggested by various authors (e.g. Aki, 1970 and Brune, 1970), with a "flat" long period level.

II. Near field behavior

In the near field, the most important term in the Hankel function is

$$h_\ell^{(2)}(k_\alpha r) \sim \frac{i(2\ell)!}{\ell!(2k_\alpha r)^\ell} \frac{e^{-ik_\alpha r}}{k_\alpha r} \qquad \omega \ll 1$$

from this we get

$$\left.\begin{array}{ll} 1)\ \underline{R_s < r} & \left[\tilde{\chi}_\alpha(\omega)\right]_N = 0(\omega) \\ 2)\ \underline{R_s = \infty} & \left[\tilde{\chi}_\alpha(\omega)\right]_N = 0\left(\frac{1}{\omega}\right) \end{array}\right\} \quad \omega << 1$$

In this case however, the displacement spectrum is worth a more detailed investigation. We have in general

$$\tilde{u}(\underline{r},\omega) = -\frac{1}{k_p^2}\ \nabla\tilde{\Theta}(\underline{r},\omega) + \frac{2}{k_s^2}\ \nabla\ x\underline{\tilde{\Omega}}(\underline{r},\omega)$$

where the first term represents the P-wave radiation, and the second the S-wave radiation. As an example we shall consider in detail, the radial component of motion.

$$\tilde{u}_r(\underline{r},\omega) = -\frac{1}{k_p^2}\frac{\partial\tilde{\Theta}}{\partial r} - \frac{2}{rk_s^2}\left\{\left(\sin\phi\ \frac{\partial}{\partial\theta} + \cos\phi\ \ \cos\theta\ \frac{\partial}{\partial\phi}\right)\tilde{\Omega}_1 + \left(\sin\phi\ \ \cos\theta\ \frac{\partial}{\partial\phi} - \cos\theta\ \frac{\partial}{\partial\theta}\right)\tilde{\Omega}_2 - \frac{\partial}{\partial\phi}\ \tilde{\Omega}_3\right\}$$

Noting that

$$\frac{\partial h_\ell^{(2)}}{\partial r}(k_\alpha r) - \frac{i(2\ell)!\ (\ell+2)\ e^{-ik_\alpha r}}{2^\ell\ \ell!\ k_\alpha^{\ell+1}\ r^{\ell+2}} \quad \omega << 1$$

We see that

$$\tilde{u}_r^{(p)}(\underline{r},\omega) = 0\left(\frac{1}{\omega^3}\right) \text{ for } \omega << 1$$

Similarly

$$\tilde{u}_r^{(s)}(\underline{r},\omega) = 0\left(\frac{1}{\omega^3}\right) \text{ for } \omega << 1$$

Such asymptotic behavior would seem to indicate that both P and S waves carry infinite energy at very long periods. Of course, the reason for this surprising behavior is that one cannot define P- and S-waves in the static limit, and that the mathematical separation indicated above is not physically realized, that is P and S energy overlaps and adds in the long period limit. In particular, we can show analytically that

$$\tilde{u}_r(\underline{r},\omega) = \tilde{u}_r^{(p)} + u_r^{(s)} = 0\left(\frac{1}{\omega}\right) \quad \text{for } \omega << 1$$

The proof is rather tedious but tractable. More importantly, numerical results exhibit the same behavior to a high degree of accuracy, and this provides a useful check on the stability and accuracy of numerical calculations.

High frequency behavior

One can show that the asymptotic behavior of the displacement spectra for all the cases considered in this report is $\tilde{u}(\omega) = 0\left(\frac{1}{\omega^3}\right)$, $\omega \to \infty$.

Numerical calculations also show this asymptotic behavior. However the preliminary investigations show that the spectra are quite complicated at high frequency, due to the significant excitation of higher order multipoles. The same complexity is present in theoretical radiation patterns as well. Because analytical investigations become extremely cumbersome for the intermediate frequency range, one has to rely on numerical parameter studies to comprehend the nature of the seismic radiation in that range. Such studies are currently underway.

Summary

We solved the problem of the relaxation of a prestressed elastic medium due to a propagating rupture for two extreme prestress conditions. The first one, where the relaxation zone is limited in size, may be used to model the effect

of a local concentration of stress. The other one, where an infinite medium is allowed to relax, models cases of high stress levels on a regional scale, and is particularly useful in the investigation of near-field effects. On the basis of these two extremes, one can bracket the long period behavior of the far field displacement spectrum

$$0(\omega^2) \leq [\tilde{u}]_F \leq 0(1) \qquad \text{for } \omega << 1$$

The lower bound corresponds to the source model previously proposed by Archambeau (1968), and yields a peaked spectrum. The upper bound gives a long period spectral shape similar to that proposed by Aki (1970) and Brune (1970).

The "near field" is defined as that part of the radiation field decaying with distance as $\frac{1}{r^n}$, $n \geq 2$. It is reasonable to assume in this case that the observers lie within the relaxation zone. Making this zone infinite in size, one finds that $[\tilde{u}]_N = 0\ (1/\omega)$ for $\omega << 1$. This merely expresses the fact that a net static displacement is to be observed.

Both of the extreme stress conditions yield average slopes of ω^{-3} for the high frequency end of the spectrum. This fact is critical when one tries to explain M_b/M_S data.

A major effort has been undertaken to add these new theoretical developments to existing computer programs. Numerical computations constitute the most efficient method of determining the effects of the different source parameters on the radiation field and the asymptotic behavior described above provides an important check on the accuracy of the numerical codes.

(2) Surface Waves from a General Elastodynamic Source in a Vertically Inhomogeneous Half-space

As our source in a locally homogeneous region, we take the slightly modified elastodynamic source form of Archambeau (1968).

$$\bar{\phi}_s = (-1/k_\alpha^2) = \sum_{n=0}^{\infty} \sum_{m=0}^{n} \left\{ A_{nm} \cos m\phi + B_{nm} \sin m\phi \right\} P_n^m(\cos\theta)\, h_n^{(2)}(k_\alpha R)$$

$$\bar{\psi}_{sj} = (2/k_\beta^2) = \sum_{n=0}^{\infty} \sum_{m=0}^{n} \left\{ C_{nm}^{(j)} \cos m\phi + D_{nm}^{(j)} \sin m\phi \right\} P_n^m(\cos\theta)\, h_n^{(2)}(k_\beta R) \qquad (1)$$

where $\bar{\phi}_s$ and $\bar{\psi}_{sj}$ are the Fourier-time transformed compressional and Cartesian shear potentials (j=1,2 and 3) respectively. In order to express these potentials in terms of the separable solutions to the Helmholtz equation in cylindrical coordinates, we use the following relation (Harkrider and Archambeau, 1973)

$$h_n^{(2)}(k_v R)\, P_n^m(\cos\theta) = \frac{(i)^{-n}}{k_v} \left[\operatorname{sgn}(h-z) \right]^{m+n} \int_0^{\infty} \bar{P}_n^m \left\{ \nu_v/k_v \right\} \frac{e^{-i\nu_v |z-h|}}{\nu_v} J_m(kr)\, k\,dk$$

where

$$\nu_v \equiv k r_v = \begin{cases} (k_v^2 - k^2)^{1/2} & ;\ k < k_v ,\ k_v = \omega/v \\ -i(k^2 - k_v^2)^{1/2} & ;\ k > k_v \end{cases}$$

$$P_n^m(\xi) \equiv (1-\xi)^{m/2}\, P_n^{(m)}(\xi)$$

$$\bar{P}_n^m(\xi) \equiv (\xi^2-1)^{m/2}\, P_n^{(m)}(\xi)$$

$$P_n^{(m)}(\xi) = \frac{d^m}{d\xi^m} P_n(\xi)$$

v is either α or β, the compression or shear velocity respectively and $(r,z) = (0,h)$ is the source location.

Making use of this relation, we can rewrite equations (1) as

$$\bar{\phi}_s = \sum_{m=0}^{n} \int_0^\infty \left\{ \bar{A}_m \cos m\phi + \bar{B}_m \sin m\phi \right\} \frac{e^{-ikr_\alpha |z-h|}}{r_\alpha} J_m(kr)\, dk \qquad (3)$$

$$\bar{\psi}_{sj} = \sum_{m=0}^{n} \int_0^\infty \left\{ \bar{C}_m^{(j)} \cos m\phi + \bar{D}_m^{(j)} \sin m\phi \right\} \frac{e^{-kr_\beta |z-h|}}{r_\beta} J_m(kr)\, dk$$

where

$$\bar{A}_m = \sum_{n=m}^{\infty} \frac{(i)^{-n}}{k_\alpha^3} \left[\operatorname{sgn}(h-z) \right]^{m+n} A_{nm} \bar{P}_n^m \left\{ \nu_\alpha / k_\alpha \right\}$$

$$\bar{B}_m = \sum_{n=m}^{\infty} \frac{(i)^{-n}}{k_\alpha^3} \left[\operatorname{sgn}(h-z) \right]^{m+n} B_{nm} \bar{P}_n^m \left\{ \nu_\alpha / k_\alpha \right\} \qquad (4)$$

$$\bar{C}_m^{(j)} = \sum_{n=m}^{\infty} \frac{(i)^{-n}}{k_\beta^3} \left[\operatorname{sgn}(h-z) \right]^{m+n} C_{nm}^{(j)} \bar{P}_n^m \left\{ \nu_\beta / k_\beta \right\}$$

$$\bar{D}_m^{(j)} = \sum_{n=m}^{\infty} \frac{(i)^{-n}}{k_\beta^3} \left[\operatorname{sgn}(h-z) \right]^{m+n} D_{nm}^{(j)} \bar{P}_n^m \left\{ \nu_\beta / k_\beta \right\}$$

Next we obtain an expression for the cylindrical SV potential, which is a convenient potential for our cylindrical coordinate system, in terms of the Cartesian SV potentials given in equation (3). The vertical displacement integrand, w, of its k integral is related to the compressional and Cartesian SV potential integrands by

$$w = \frac{\partial \phi}{\partial z} + \frac{\partial \psi_2}{\partial x} - \frac{\partial \psi_1}{\partial y} \tag{5}$$

and in terms of the compressional and SV potential integrands by

$$w = \frac{\partial \phi}{\partial z} + k^2 \psi \tag{6}$$

which by inspection yields the relation

$$\psi = \frac{1}{k^2} \left(\frac{\partial \psi_2}{\partial x} - \frac{\partial \psi_1}{\partial y} \right) \tag{7}$$

Performing the above operation and comparing with the cylindrical SV potential

$$\bar{\psi}_s = \sum_{m=0}^{n} \int_0^{\infty} \left\{ \bar{E}_m \cos m\phi + \bar{F}_m \sin m\phi \right\} \frac{e^{-ikr_\beta |z-h|}}{r_\beta} J_m(kr)\, dk \tag{8}$$

we obtain the following relation between coefficients as derived in (Harkrider and Archambeau, 1973).

$$\begin{aligned} 2k\bar{E}_m &= \left(\bar{C}^{(2)}_{m+1} - C^{(2)}_{m-1} \right) - \left(\bar{D}^{(1)}_{m+1} + \bar{D}^{(1)}_{m-1} \right) \\ 2k\bar{F}_m &= \left(\bar{C}^{(1)}_{m+1} + \bar{C}^{(1)}_{m-1} \right) + \left(\bar{D}^{(2)}_{m+1} - \bar{D}^{(2)}_{m-1} \right) \end{aligned} \qquad 1 < m \leq n \tag{9}$$

where

$\bar{C}^{(j)}_m$ and $\bar{D}^{(j)}_m$ are zero for $m > n$ and $m < 0$,

and in addition

$$\bar{C}_0^{(2)} = \bar{D}_0^{(1)} \qquad , \qquad \bar{C}_0^{(1)} = -\bar{D}_0^{(2)}$$

and

$$\bar{F}_0 = 0.$$

The cylindrical source potentials given by equations (3) and (8) may now be substituted into the multilayer formulation of Harkrider (1964). But first we note that alternating terms in the infinite series in equations (4) are of opposite sign depending on whether z is greater or lesser than h. We separate the series such that

$$\bar{A}_m = \bar{A}_m^e + \bar{A}_m^o \tag{10}$$

where the e superscript denotes a new series made up of the terms with m+n even and the o, a series formed by terms with m+n odd. A similar separation is done for the other source coefficients. The new coefficients have the following property

$$\bar{A}_m^e(z > h) = \bar{A}_m^e(z < h)$$

and (11)

$$\bar{A}_m^o(z > h) = -\bar{A}_m^o(z < h)$$

Defining

$$\delta U_m = \delta \left(\frac{\dot{u}_s}{c} \right)_m^c \cos m\phi + \delta \left(\frac{\dot{u}_s}{c} \right)_m^s \sin m\phi$$

$$\delta W_m = \delta \left(\frac{\dot{w}_s}{c} \right)_m^c \cos m\phi + \delta \left(\frac{\dot{w}_s}{c} \right)_m^s \sin m\phi$$

$$\delta Z_m = \delta \sigma_m^c \cos m\phi + \delta \sigma_m^s \sin m\phi$$

$$\delta X_m = \delta \tau_{Rm}^c \cos m\phi + \delta \tau_{Rm}^s \sin m\phi \qquad (12)$$

$$\delta V_m = \delta \left(\frac{\dot{v}_s}{c} \right)_m^c \cos m\phi + \delta \left(\frac{\dot{v}_s}{c} \right)_m^s \sin m\phi$$

$$\delta Y_m = \delta \tau_{Lm}^c \cos m\phi + \delta \tau_{Lm}^s \sin m\phi$$

and comparing our source potential relations with equations (30) and (37) in Harkrider (1964), we obtain

$$\delta\left(\frac{\dot{u}_s}{c}\right)_m^c = 2k^2\left[\frac{\overline{A}_m^o}{r_\alpha} - ik\,\overline{E}_m^e\right]$$

$$\delta\left(\frac{\dot{u}_s}{c}\right)_m^s = 2k^2\left[\frac{\overline{B}_m^o}{r_\alpha} - ik\,\overline{F}_m^e\right]$$

$$\delta\left(\frac{\dot{w}_s}{c}\right)_m^c = 2k^2\left[\overline{A}_m^e + ik\,\frac{\overline{E}_m^o}{r_\beta}\right] \qquad (13)$$

$$\delta\left(\frac{\dot{w}_s}{c}\right)_m^s = 2k^2\left[\overline{B}_m^e + ik\,\frac{\overline{F}_m^o}{r_\beta}\right]$$

$$\delta\sigma_m^c = 2\rho c^2k^2\left[(\gamma-1)\,\frac{\overline{A}_m^o}{r_\alpha} - ik\gamma\,\overline{E}_m^e\right]$$

$$\delta\sigma_m^s = 2\rho c^2k^2\left[(\gamma-1)\,\frac{\overline{B}_m^o}{r_\alpha} - ik\gamma\,\overline{F}_m^e\right]$$

$$\delta\tau_{Rm}^c - 2\rho c^2k^2\left[-\gamma\overline{A}_m^e - ik(\gamma-1)\,\frac{\overline{E}_m^o}{r_\beta}\right]$$

$$\delta\tau_{Rm}^s = 2\rho c^2k^2\left[-\gamma\overline{B}_m^e - ik(\gamma-1)\,\frac{\overline{F}_m^o}{r_\beta}\right]$$

$$\delta\left(\frac{\dot{v}_s}{c}\right)_m^c = i2k^2 \frac{\bar{C}_m^{(3)o}}{r_\beta}$$

$$\delta\left(\frac{\dot{v}_s}{c}\right)_m^s = i2k^2 \frac{\bar{D}_m^{(3)o}}{r_\beta}$$

$$\delta\tau_{Lm}^c = - i2k^2\mu \bar{C}_m^{(3)e}$$

$$\delta\tau_{Lm}^s = - i2k^2\mu \bar{D}_m^{(3)e}$$

Following Harkrider (1964) we obtain as our integral solution for the vertical displacement at the surface of our inhomogeneous half-space

$$\langle w_o \rangle = \sum_{m=0}^{n} \int_0^\infty \left(\frac{1}{ik}\right) \frac{R_{11}[A]_m - R_{12}[B]_m + R_{13}Z_m}{F_e} J_m(kr)\, dk \qquad (14)$$

where

$$F_e = - R_{11} - [T]R_{12}$$

$$[T] = \left[\frac{\sigma_o}{\dot{w}_o/c}\right]$$

$$[A]_m = \left[-(A_{RS})_{43}\ \delta U_m + (A_{RS})_{33}\ \delta W_m - (A_{RS})_{23}\ \delta Z_m + (A_{RS})_{13}\ \delta X_m \right]$$

$$[B]_m = \left[(A_{RS})_{42}\ \delta U_m - (A_{RS})_{32}\ \delta W_m + (A_{RS})_{22}\ \delta Z_m - (A_{RS})_{12}\ \delta X_m \right] \qquad (15)$$

and

$$Z_m = \left[-(A_{RS})_{41}\ \delta U_m + (A_{RS})_{31}\ \delta W_m - (A_{RS})_{21}\ \delta Z_m + (A_{RS})_{11}\ \delta X_m \right]$$

(For symbols used without definition here, refer to Harkrider (1964), (1970) and Harkrider and Flinn (1970).

The matrix A_{RS} as defined in Harkrider (1964) is the layer product matrix which gives the displacement-stress vector associated with P-SV motion at source depth in terms of the surface displacement-stress vector. The integral solution given by equation (14) is also valid for a vertically inhomogeneous half-space where A_{RS} is the linear transformation of the P-SV displacement stress vector from the surface down to the source. The only restriction on this form of the solution is that at some depth the media is terminated by a homogeneous half-space.

The surface azimuthal displacement due to SH waves is given by

$$\langle v_o \rangle = -\sum_{m=0}^{n} \int_0^{\infty} \left(\frac{1}{ik}\right) \frac{N_m^{(1)} N_m^{(2)}}{F_L} \frac{dJ_m(kr)}{d(k_m)}\, dk \qquad (16)$$

where

$$F_L = -(A_L)_{21}^{*} - (A_L)_{11} \mu_\ell\ r_{\beta\ell}^{*}$$

$$N_m^{(1)} = i\left[(A_L)_{22} - (A_L)_{12}^{*} \mu_\ell\ r_{\beta\ell}^{*} \right]\left[(A_{LS})_{11}\ \delta Y_m - (A_{LS})_{12}\ \delta V_M \right] \qquad (17)$$

and

$$N_m^{(2)} = 1 + \frac{F_L}{N_m^{(1)}} \left[(A_{LS})_{12}\ \delta Y_m - (A_{LS})_{22}\ \delta V_m \right]$$

The A_{LS} is the transfer matrix for the displacement stress vector associated with SH motion down from the surface to the source depth. A_L is the transfer matrix from the surface down to the depth at which the terminating homogeneous half-space begins with elastic properties denoted by subscript ℓ.

Evaluating the residue contributions of equations (14) and (16), in order to obtain the surface displacements due to Rayleigh and Love waves respectively, yields

$$\left\{w_o\right\} = i\,\frac{\pi}{k}\,\underline{A}_R \sum_{m=0}^{n} \left\{ \delta U_m \left[\frac{\tau_{RS}(h)}{\dot{w}_o/C_R}\right] - \delta W_m \left[\frac{\sigma_s(h)}{\dot{w}_o/C_R}\right] + \delta Z_m \left[\frac{\dot{w}_s(h)}{\dot{w}_o}\right] - \delta X_m \left[\frac{\dot{u}_s(h)}{\dot{w}_o}\right] \right\} \cdot H_m^{(2)}(kr) \tag{18}$$

where

$$\underline{A}_R = -\frac{R_{12}^*}{\left(\frac{\partial F_e}{\partial k}\right)_\omega}$$

and

$$\left\{v_o\right\} = -\frac{\pi}{k^2}\,\underline{A}_L \sum_{m=0}^{n} \left\{ \delta Y_m \left[\frac{v_s(h)}{v_o}\right] - \delta V_m \left[\frac{\tau_{LS}(h)}{v_o/C_i}\right] \right\} \frac{dH_m^{(2)}(kr)}{dr} \tag{19}$$

where

$$\underline{A}_L = \frac{1}{(A_L)_{11}\left(\frac{\partial F_L}{\partial k}\right)_\omega}$$

Using equations (13) the solutions can be written as

$$\left\{ w_o \right\} = - 4\pi k_R \mu \, \underline{A}_R \left\{ K_R \phi^e - k L_R \psi^e - \frac{i}{2\mu r_\alpha} M_R \phi^o + \frac{ik}{2\mu r_\beta} N_R \psi^o \right\} \tag{20}$$

and

$$\left\{ v_o \right\} = 2\pi i \mu \, \underline{A}_L \left\{ \overline{\chi}^e \left[\frac{\dot{v}_s(h)}{\dot{v}_o} \right] + i \frac{\overline{\chi}^o}{r_\beta} \left[\frac{\tau^*_{LS}(h)}{\dot{v}_o / C_L} \right] \right\} \tag{21}$$

where

$$K_R = \left[\frac{\dot{u}^*_s(h)}{\dot{w}_o} \right] - \frac{1}{2\mu} \left[\frac{\sigma^*_s(h)}{\dot{w}_o / C_R} \right]$$

$$L_R = \left[\frac{\dot{w}_s(h)}{\dot{w}_o} \right] + \frac{1}{2\mu} \left[\frac{\tau_{RS}(h)}{\dot{w}_o / C_R} \right] \tag{22}$$

$$M_R = \rho C^2 (\gamma - 1) \left[\frac{\dot{w}_s(h)}{\dot{w}_o} \right] + \left[\frac{\tau_{RS}(h)}{\dot{w}_o / C_R} \right]$$

$$N_R = \rho C^2 (\gamma - 1) \left[\frac{\dot{u}^*_s(h)}{\dot{w}_o} \right] - \left[\frac{\sigma^*_s(h)}{\dot{w}_o / C_R} \right]$$

$$\gamma = \frac{2\beta^2}{C^2}$$

$$\phi^e = \sum_{m=0}^{n} \left(\overline{A}^e_m \cos m\phi + \overline{B}^e_m \sin m\phi \right) H^{(2)}_m (kr)$$

$$\psi^e = \sum_{m=0}^{n} \left(\overline{E}^e_m \cos m\phi + \overline{F}^e_m \sin m\phi \right) H^{(2)}_m (kr)$$

$$\bar{\chi}^{e} = \sum_{m=0}^{n} \left(\bar{C}_m^{(3)e} \cos m\phi + \bar{D}_m^{(3)e} \sin m\phi \right) \frac{dH^{(2)}}{dr} (kr)$$

and the o superscripted variables defined similarly.

(3) Near Field Wave Propagation in Layered Media using Simple Dislocation and Explosion Sources.

We begin by first reviewing the treatment of a spherically symmetrical source followed by the general treatment of dislocation models. Our approach is to develop the mathematical tools for a very simple model, an infinite homogeneous medium, that can be used in treating the "n" layer model after the application of generalized ray theory. To apply generalized ray theory we must reduce all sources to simple displacement potentials of the P, SV, and SH type. This is easily accomplished for symmetric sources like explosions but difficult for earthquake sources. We will present such potentials later.

The radial displacement for a simple point source can be expressed in terms of the potential

$$U_R(R,t) = \frac{\partial}{\partial R}\,\phi(t - \frac{R}{V}) \tag{1}$$

where

$$\phi(R,t) = \psi_o\,\delta(t - R/V)/R. \tag{2}$$

R is the radial coordinate and V is the velocity. The parameter ψ_o is a constant with units of volume (assumed to be unity) and we are assuming a delta function time history. Taking the Laplace transform of (2) yields

$$\bar{\phi}(R,s) = \frac{e^{-\frac{R}{V}s}}{R} \quad . \tag{3}$$

Applying the Sommerfeld transformation we can write $\bar{\phi}$ in terms of cylindrical coordinates

$$(4) \quad \bar{\phi}(r,z,s) = \int_0^\infty \frac{J_o(kr)\, e^{-\left(k^2 + \frac{s^2}{v^2}\right)^{1/2} |z|}\, kdk}{\left(k^2 + \frac{s^2}{v^2}\right)^{1/2}}$$

where k is the horizontal wave number. Next we go from J_o to K_o (modified Bessel function) using the basic Cagniard-de Hoop notation

$$k = -isp$$

and

$$(5) \quad \phi(r,z,s) = \frac{2}{\pi}\, s\, Im \int_0^{i\infty} \frac{p}{\eta_V}\, K_o(spr)\, e^{-s\,\eta_V |z|}\, dp$$

where $\eta_V = \left(\frac{1}{V^2} - p^2\right)^{1/2}$.

Now we must take the inverse Laplace transform, in general we will be working with $K_n(spr)$ so we will allow n to be unspecified for the moment. Equation (5) can be solved exactly but there are some useful approximations to discuss. Using the asymptotic expansion (9.7.2 Abramowitz and Stegun) we have

$$(6) \quad K_n(x) = \left(\frac{\pi}{2x}\right)^{1/2} e^{-x} \left[1 + \frac{\mu-1}{8x} + \frac{(\mu-1)(\mu-9)}{2(8x)^2} + \ldots\ldots\right]$$

where $\mu = 4n^2$. The series converges the fastest for small values of n. However, assuming n = 2 (the highest order needed in dislocation modeling) and x = 3 we get

$$K_2(3) = \left(\frac{\pi}{6}\right)^{1/2} e^{-3} \left[1 + .623 + .091\right] \quad .$$

This approximation is 98% accurate.

If we assume large (spr) we have

$$(7) \qquad K_o(spr) \approx \left(\frac{\pi}{2spr}\right)^{1/2} e^{-spr}$$

and substituting into (5) we obtain

$$(8) \quad \phi(v,z,s) = \left(\sqrt{\frac{2}{r\pi}}\right) \frac{s}{\sqrt{s}} \, Im \int_0^{i\infty} \frac{\sqrt{p}}{\eta_V} e^{-(pr + \eta_V|z|)s} \, dp$$

which can be treated by line source theory.

Following the de Hoop transformation

$$t = pr + \eta_V z \qquad z > 0$$

we obtain

$$p = \frac{r}{R^2} t + \left(\frac{R^2}{V^2} - t^2\right)^{1/2} \frac{z}{R^2} \, , \; t < \frac{R}{V}$$

$$(9)$$

$$p = \frac{r}{R^2} t + i\left(t^2 - \frac{R^2}{V^2}\right)^{1/2} \frac{z}{R^2} \, , \qquad t \geq \frac{R}{V}$$

The asymptotic solution becomes

$$(10) \qquad \phi(r,z,t) = \sqrt{\frac{2}{r}} \frac{\partial}{\partial t} \left[\frac{1}{\sqrt{t}} * Im \left(\frac{\sqrt{p}}{\eta_V} \frac{dp}{dt} \right) \right]$$

where

$$\frac{dp}{dt} = \frac{i\eta_V}{\left(t^2 - \frac{R^2}{V^2}\right)^{1/2}} \, , \qquad t \geq R/V$$

If we let $\sin h = \frac{r}{R}$ and $\cos h = \frac{z}{R}$ (see diagram below)

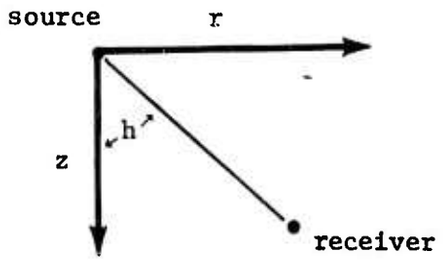

we obtain

$$(11) \qquad p = \frac{\sin h}{R} t + i \left(t^2 - \frac{R^2}{V^2} \right)^{1/2} \frac{\cos h}{R}$$

and

$$(12) \qquad \eta_V = \frac{\cos h}{R} t - i \left(t^2 - \frac{R^2}{V^2} \right)^{1/2} \frac{\sin h}{R}$$

Equation (10) is to be evaluated along the contour defined by (9). A further simplication of (10) can be obtained by making a so called "first-motion" approximation. For values of t near R/V, $p \approx \frac{\sin h}{V}$ and $\eta_V = \frac{\cos h}{V}$ and (10) reduces to

$$(13) \qquad \phi(r,z,t) \approx \frac{1}{R} \delta\left(t - \frac{R}{V} \right) \quad ,$$

which was the starting equation (2). Note that $p = \frac{\sin h}{V}$ (the ray parameter) in the first-motion approximation. This approximation is useful for comparing Cagniard solutions of dislocation models with conventional far-field results.

The exact solution of (5) can be obtained by applying transform theory. We note that

$$(14) \qquad L^{-1}\left[K_n(spr) \right] = \frac{H(t - pr)\, \cos h \left(n \cosh^{-1}\left(\frac{t}{pr}\right)\right)}{\left((t^2 - (pr)^2\right)^{1/2}}$$

and applying the shift rule

$$L^{-1}\left[e^{-as} f(s) \right] = F(t-a)\, H(t-a)$$

then

$$(15) \qquad L^{-1}\left[K_n(spr)\, e^{-gs} \right] = \frac{H(t - pr - g)\, \cosh\left(n \cosh^{-1}\left(\frac{t-g}{pr}\right)\right)}{\left((t-g)^2 - (pr)^2 \right)^{1/2}}$$

where $g = \eta_V z$,

Let $\tau = pr + \eta_V z$

$$(t - \eta z)^2 - (pr)^2 = (t-r)(t-\tau + 2pr)$$

And let

$$C(t,p(r)) \equiv \cosh\left(n \cosh^{-1}\left(\frac{t-\eta_V z}{pr}\right)\right)$$

$$\frac{t-\eta_V z}{pr} = \left[\frac{t - \tau + pr}{pr}\right]$$

The solution then becomes

$$(16) \qquad \phi(v,z,t) = \frac{2}{\pi}\frac{\partial}{\partial t}\ Im \int^{t} \frac{C(t,\tau)}{(t-\tau)^{1/2}\ (t - \tau + 2pr)^{1/2}} \frac{dp}{d\tau}\frac{p(\tau)}{\eta_V}\, d\tau \ .$$

The integral for various values of t can be evaluated using the transformations used by Helmberger (1968).

Earthquake sources

In this section we will examine some relatively simple dislocation models. Starting with Haskell's representation for shear faulting it is relatively easy to devise the displacements for double couples in an infinite medium. The solution for a strike-slip fault becomes

$$\bar{W}(r,z,\omega) = K\left[\frac{\partial}{\partial z}\left(\frac{\partial^2 A}{\partial r^2} - \frac{1}{r}\frac{\partial A}{\partial r}\right)\right] \sin 2\theta$$

$$\bar{V}(r,z,\omega) = K\left[\frac{2}{r}\left(\frac{\partial^2 A}{\partial r^2} - \frac{1}{r}\frac{\partial A}{\partial r}\right) + k_\beta^2 \frac{\partial B}{\partial r}\right] \cos 2\theta$$

$$\bar{q}(r,z,\omega) = K\left[\frac{\partial}{\partial r}\left(\frac{\partial^2 A}{\partial r^2} - \frac{1}{r}\frac{\partial A}{\partial r}\right) + k_\beta^2 \frac{\partial B}{\partial r}\right] \sin 2\theta$$

where W, V and q are the displacements in the vertical, azimuthal and radial coordinates. The parameters are

$$A = \frac{e^{-i\omega \frac{R}{\beta}}}{R} - \frac{e^{-i\omega \frac{R}{\alpha}}}{R}$$

$$B = e^{-i\omega \frac{R}{\beta}}$$

and

$$K = -\frac{\mu\, LW\bar{D}(\omega)}{4\pi\omega^2\rho}, \quad k_\beta = \frac{\omega}{\beta} \quad .$$

$\bar{D}(\omega)$ is the Fourier transform of the time history across the fault. We are assuming an instantaneous motion over a rectangle with dimensions LH. It is easy to generalize to finite rupture velocity by adding the moving source directivity (see Mikumo, 1972). We will add such features later along with multiple sources as well. Our approach is to compute and understand the three basic faults, strike-slip, dip-slip and 45° dip slip. Burridge and Knopoff (1964) show that a linear combination of these three solutions will represent any fault orientation. We will treat the strike-slip dislocation as an example although any motion can be handled using our approach.

Next, we breakdown these displacements in terms of potentials,

$$\bar{W} = \frac{\partial \bar{\phi}}{\partial z} + \frac{\partial^2 \bar{\psi}}{\partial z^2} + k_\beta^2 \bar{\psi}$$

$$\bar{V} = \frac{1}{r}\frac{\partial \phi}{\partial \theta} + \frac{1}{r}\frac{\partial^2 \bar{\psi}}{\partial z \partial \theta} - \frac{\partial \bar{\chi}}{\partial r} \qquad (17)$$

$$\bar{q} = \frac{\partial \bar{\phi}}{\partial r} + \frac{\partial}{\partial r}\frac{\partial \bar{\psi}}{\partial z} + \frac{1}{r}\frac{\partial \bar{\chi}}{\partial \theta}$$

After some effort the potentials become

$$\bar{\phi} = -K \int_0^\infty k^2 F_\alpha J_2(kr) \sin 2\theta \, dk$$

$$\bar{\psi} = K \frac{\partial}{\partial z} \int_0^\infty F_\beta J_2(kr) \sin 2\theta \, dk \qquad (18)$$

$$\bar{\chi} = K k_\beta^2 \int_0^\infty F_\beta J_2(kr) \cos 2\theta \, dk$$

where

$$F_V = \frac{k\, e^{-(k^2-K_V^2)^{1/2}|z|}}{(k^2-K_V^2)^{1/2}} \tag{19}$$

We are concerned with the evaluation of the integrals in (18), so we need only consider the field variable:

$$\bar{\zeta}(r,z,\omega) \equiv -\int_0^\infty F_V\, J_2(kr)\, dk \quad . \tag{20}$$

Changing variables

$$\omega = -is \text{ and } k = -isp$$

we obtain

$$\bar{\zeta}(r,z,s) = \frac{2}{\pi} s\, \mathrm{Im} \int_0^{i\infty} \frac{p}{\eta_V} K_2(spr)\, e^{-s\eta_V z}\, dp \tag{21}$$

where

$$\eta_V = \left(\frac{1}{V^2} - p^2\right)^{1/2} \quad .$$

Equation (21) is almost identical to (5) of the previous section and can be solved following the same technique. Since K_2 decays slower than K_o we know that $\bar{\zeta}$ will develop a tail. That is, the polarity of the second term of the series given in equation (6) is negative for n = 0 and positive for n = 2 indicating a long period enhancement. Suppose we express ζ in a series

$$\zeta = \zeta_1 + \zeta_2 + \zeta_3$$

where the ζ's indicate the various terms in this expansion;

$$\zeta_1 = \frac{2}{\pi}\frac{\partial}{\partial t}\left[\frac{1}{\sqrt{t}} * J_1(t)\right]$$

$$J_1 = Im\left(\frac{\sqrt{p}}{\eta_V}\frac{dp}{dt}\right)\frac{1}{\sqrt{2r}}$$

(22)

$$\zeta_2 = \left(\frac{15}{8}\right)\frac{2}{\pi}\left[\frac{1}{\sqrt{t}} * J_2(t)\right]$$

$$J_2 = Im\left(\frac{\sqrt{p}}{\eta_V}\frac{dp}{dt}\cdot\frac{1}{p}\right)\frac{1}{\sqrt{2r^3}}$$

and

$$\zeta_3 = \frac{105}{128}\left(\frac{2}{\pi}\right)\int dt\left[\frac{1}{\sqrt{t}} * J_3(t)\right]$$

$$J_3 = Im\left(\frac{\sqrt{p}}{\eta_V}\frac{dp}{dt}\frac{1}{p^2}\frac{1}{(2r^5)^{1/2}}\right)$$

This series can be readily evaluated and is applicable for all periods such that

$$T < \frac{2\pi r}{3V}$$

For small distances and long periods we must use expressions similar to (16). Before generalizing to a layered half space we will consider the first-motion approximations of the equations given by (18). First we note that

$$\zeta \simeq \zeta_1 = \frac{1}{R}\,\delta\left(t - \frac{R}{V}\right) \qquad \text{where}$$

$p = \frac{\sinh}{V}$ and $\eta_V = \frac{\cosh}{V}$, as indicated from the first section. We can then write

$$\phi(r,z,s) \approx + \frac{\mu\ LHD(s)}{4\pi\rho\ s^2}\ (s^2p^2)\ L\left[\frac{\delta(t - \frac{R}{\alpha})}{R}\right] \sin 2\theta$$

(23)

$$\phi(r,z,t) = \frac{\beta_o^2(LHD_o)}{4\pi}\left(\frac{\sinh}{\alpha}\right)^2 \frac{H(t-R/\beta)}{R} \sin 2$$

assuming $D(s) = D_o/s$, that is we assume a step function time history of the displacement across the fault. The moment is just $\mu(LHD_o)$.

Similarly,

$$(24) \qquad \chi(r,z,t) = - \frac{\beta_o^2(LHD_o)}{4\pi} \cdot\left(\frac{1}{\beta_o^2}\right) \frac{H(t-R/V)}{R} \cos 2\theta$$

It is convenient to define a new potential $\bar{\psi}^1 = \frac{s}{\beta}\,\bar{\psi}$ which reduces to

$$(25)\ \psi^1(r,z,t) = - \frac{\beta_o^2(LHD_o)}{4\pi}\left(\frac{\cos h}{\beta_o^2}\right) \frac{H(t-R/B)}{R} \sin 2\theta$$

where we used $\eta_\beta = \frac{\cos h}{\beta}$.

These first-motion approximations can be compared with the results of geometrical ray theory by computing the displacement due to P and SV and SH waves where

$$(26) \qquad \bar{U}_p = \left(w_\phi^2 + q_\phi^2\right)^{\frac{1}{2}}$$

$$(27) \qquad \overline{U}_{SV} = \left(w_\psi^2 + q_\psi^2\right)^{\frac{1}{2}}$$

$$(28) \qquad U_{SH} = V_\chi$$

For example, note that the operations can be written

$$L^{-1}\left[\frac{\partial}{\partial r}\,\zeta(r,z,s)\right] = -\,L^{-1}\left((sp)\zeta\right)$$

$$L^{-1}\left[\frac{\partial}{\partial z}\,\zeta(r,z,s)\right] = -\,L^{-1}\left[s\eta_V\zeta\right]$$

and using the definitions (17) we have

$$\overline{U}_p(r,z,\tau) = \beta_o^2\left(\frac{LHD_o}{4\pi}\right)\left(\frac{\sin^2 h}{\alpha^3}\right)\frac{\delta(t-R/\alpha)}{R}\sin 2\theta$$

$$= \left(\frac{\beta^2}{\alpha^2}\right)\left(\frac{LHD_o}{2\pi\alpha}\right)\frac{R(h,\theta)}{}\,\frac{\delta(t-R/\alpha)}{R}$$

where

$$R(h,\theta) = \frac{\sin^2 h \sin 2\theta}{2}$$

This is the far-field expression for the field given by Ben-Menahem, Smith and Teng (1965).

The form of the solution to use is dictated by the value of r, the source time history and the model response. It would appear that all three solutions, exact integral evaluation given by (16), the power series development (22), and the first-motion approximation, have domains of interest. We are primarily interested in the first two, especially the power series solution for application to the near field radiation field observations.

Generalization to layered half space

Using the method of generalized rays we can construct solutions by the same technique as used for the case of no azimuthal dependence. We will not list all the expressions here but we will work out the equations for the ϕ-potential as an example. For an incident P-wave at the free surface we have

$$\bar{\phi}(r,z,\theta,s) = M_o\left(\frac{2}{\pi}\right) Im \int p^2 \, F_\alpha(r) \, G_\phi(z) \sin 2\theta \, dp$$

where

$$G_\phi(z) = e^{-s\eta_\alpha |z_o|} + R_{pp} \, e^{-s\eta_\alpha z_o}$$

$$F_\alpha(r) = \frac{p}{\eta_\alpha} K_2(spr)$$

$$M_o = \beta^2\left(\frac{LHD_o}{4\pi}\right)$$

and the time history across the fault is assumed to be a step function in displacement. The sources is situated at z_o. There will also be a converted SV wave which can be written

$$\bar{\psi}^1(r,z,\theta,s) = M_o\left(\frac{2}{\pi}\right) Im \int p^2 \left(F_\alpha(r) G_\psi(z) \sin 2\theta\right) dp$$

where

$$G_\psi = \frac{1}{\beta p} R_{ps} \, e^{-s\eta_\alpha z_o}$$

If one substitutes these equations into the stress equation, the zero stress conditions at the boundary are satisfied. The vertical displacement becomes

$$\overline{w}_{\phi}(r,z,\theta,s) = M_o \frac{2}{\pi} s \; Im \int_0^{i\infty} p^2 \; M(\alpha) \; RPZ \sin 2\theta \; dp$$

where

$$M(v) = \frac{p}{\eta_V} \left[K_1(spr) + \frac{2}{spr} K_2(spr) \right]$$

and

$$RPZ = \frac{2\eta_\alpha \; (\eta_\beta^2 - p^2)}{\beta^2 \; R(p)}$$

with

$$R(p) = (\eta_\beta^2 - p^2) \; + 4 \; p^2 \eta_\alpha \eta_\beta .$$

R(p) is just the Rayleigh denominator. The radial displacement produced by the ϕ potential becomes

$$\overline{q}_{\phi}(r,z,\theta,s) = M_o \left(\frac{2}{\pi}\right) s \; Im \int_0^{i\infty} (p^2) \; M(\alpha) \; RPR \sin 2\theta \; dp$$

where

$$RPR = \frac{4 \; p\eta_\alpha \eta_\beta}{\beta^2 R(p)} .$$

There will also be a tangential component generated by this ϕ potential since it contains a "θ" dependence,

$$\overline{V}_{\phi}(r,z,\theta,s) = M_o \left(\frac{2}{\pi}\right) \frac{1}{r} \; Im \int_0^{i\infty} (p^2) \; RPT \; (2 \cos 2\theta) \; M_\alpha(r) \; dp$$

where

$$RPT = 1 + R_{PP} - \beta\eta_\beta R_{PS} .$$

The reflection coefficients R_{pp} and R_{PS} are given in Helmberger (1968). The various receiver functions RPZ, RPR and RPT all contain the Rayleigh denominator and thus there will be a Rayleigh wave propagating along with motion in all three coordinates. These solutions can be transformed back to the time domain by breaking the solution into far and near fields denoted WF_ϕ and WN_ϕ ,etc. Applying the theory developed in previous sections we obtain

$$WF_\phi(r,z,\theta,t) = M_o \frac{2}{\pi} \frac{\partial}{\partial t} \int^t (p^2)\ RPZ\ N(1,\tau,t)\ d\tau\ \sin 2\theta$$

where

$$N(n,\tau,t) = \frac{\cosh\ (n \cosh^{-1}\ (t-\tau + pr)/pr))}{(t-\tau)^{1/2}\ (t-\tau + 2pr)^{1/2}}$$

and for the near field we obtain

$$WN_\phi(r,z,\theta,t) = M_o\left(\frac{2}{\pi}\right)\ Im \int^t (p^2)\left(\frac{2}{pr}\right) RPZ\ \sin 2\theta\ N(2,t,\tau)\ d\tau.$$

It is useful to examine the high frequency solution by expanding M(V)

$$M(V) \approx \frac{p}{\eta_V}\sqrt{\frac{\pi}{2spr}}\ e^{-spr}\left(1 + \frac{5}{2spr} + H.O.\right)$$

Let

$$w_\phi(r,z,\theta,t) \approx (w^1{}_\phi(r,z,t) + w^2{}_\phi(r,z,t))\ \sin 2\theta$$

and

$$w^1_\phi(r,z,t) = M_o \frac{2}{\pi} \frac{\partial}{\partial t} \left[\frac{1}{\sqrt{t}} * JW^1_\phi \right]$$

where

$$JW^1_\phi = Im \left[J^1 \; p^2 \; RPZ \right]$$

and

$$J^1 = \frac{\sqrt{p}}{\eta_\alpha} \left(\frac{dp}{dt} \right) \frac{1}{\sqrt{2r}} \quad .$$

The second term is simply

$$W^2_\phi(r,z,t) = M_o \frac{2}{\pi} \left[\frac{1}{\sqrt{t}} * JW^2_\phi \right]$$

where

$$JW^2_\phi = (JW^1_\phi) \frac{5}{2pr} \quad .$$

The interpretation of these equations is relatively simple. If one neglects p^2 RPZ in JW^1_ϕ, we obtain for W^1_ϕ a delta function time response multiplied by the source strength M_o and divided by the distance traveled. The time function is the derivative of the source time function. The p^2 factor is a source correction for take-off angle as mentioned earlier. The RPZ function is equal to 2 at vertical incidence, which is the plane wave surface effect (Knopoff, Fredericks, Gangi and Porter (1957)). This function yields the Rayleigh wave at $p = \frac{1}{V_R}$, where V_R is the Rayleigh velocity. The time function will look like the derivative of a Gaussian function. The second term W^2_ϕ will also contain a Rayleigh wave but will appear as a Gaussian and decay $1/r$ faster.

The displacements produced by the other potentials χ and ψ can be computed following the same procedure. A complete presentation in matrix form will be given later. To generalize to "n" layers we need only apply the concepts of generalized reflections and transmission coefficients.

References

Ben-Menahem, A. and S. W. Smith, and T. Teng (1965). A procedure for source studies from spectrums of long-period seismic body waves, Bull. Seism. Soc. Am., 55, 203-235.

Burridge, R., and L. Knopoff (1964). Body force equivalents for seismic dislocations, Bull. Seism. Soc. Am., 54, 1875-1888.

Helmberger, D. V. (1968). The crust-mantle transition in the Bering Sea, Bull. Seism. Soc. Am., 58, 179-214.

Knopoff, L. and R. W. Fredricks, A. F. Gangi and L. P. Porter (1957). Surface amplitudes of reflected body waves.

Mikumo, T. (1971). Source process of deep and intermediate earthquakes as inferred from long-period P and S waveforms, Jour. of Phys. of the Earth, 19, 303-319.

IV. Summary of Theoretical Source Predictions: Implications for Discrimination of Earthquakes and Explosions

In this section the preliminary applications of the theoretical results of section III are summarized in terms of their relevance to discrimination of earthquakes and explosions. Additional work under a separate program (AFOSR Contract F44620-72-C-0078, Seismic Phenomena Connected with Earthquakes and Explosions) aimed at a systematic modeling of both earthquakes and explosions for purposes of defining and understanding discrimination criteria is also underway and to some extent the work reported in this section overlaps work under this second program. However, the work here is distinct in the sense that we have concentrated on the near field and the more complex problems related to observations in this range while in the former program we are mainly concerned with the far field "teleseismic" radiation. Nevertheless our investigations of the near field and the attempt to incorporate complex source models within the various wave propagation programs for studies in the near field range have resulted in a more complete understanding of earthquake radiation and the underlying basis for discrimination.

In particular, theoretical methods were devised which enabled us to express the complicated source models of Section III-1. above as equivalent point (multipolar) sources. (These methods apply to both analytical source models and numerical source models.) The approach was first utilized to combine explosive source models and the tectonic release effects together, and then to incorporate this composite source into a wave propagation program for both surface and body waves (ray theoretic approximation) so that we are able to predict the teleseismic radiation of first and later arrival body waves (including surface reflections) and Love and Rayleigh surface waves at any point in or on the earth. The same procedure was followed for earthquake sources in the present program, wherein a variety of complex relaxation source models are included and for which the teleseismic radiation fields of body waves and surface waves can be predicted at any spatial point and in either the frequency or time domains. The very near field wave propagation is handled using the Cagniard method. This approach gives results directly in the time domain.

Spectra can also be obtained from these results.

Using this predictive capability, we began a systematic investigation of the radiation fields from the variety of source representations described in Section III in order to determine the spectral characteristics of teleseismic signals from these sources and to compare these spectral predictions with observations. Our purpose was to obtain the best model (or model series) for earthquakes using data from events in various environments. Secondly, we wanted to determine the spectral details for a number of particular seismic phases, in particular, the first arriving P and pP phases (separately and combined) and the Love and Rayleigh surface waves for these "best" models. Some of the more important results were as follows:

(a) Earthquakes appear to be reasonably well modeled by relaxation source models in that, of the rather incomplete set of spectral observations made, we can obtain a reasonable fit to any of the data. In particular, either flat appearing or strongly peaked appearing spectra can be fit by the model by choice of a larger prestrained region or small prestrained region relative to the failure or fault zone dimension, so that quite different looking spectral observations can be fit by the same basic model. Indeed, the model actually predicts that a rather wide range of possibilities for the radiation field spectra are to be reasonably expected. However, we will have to wait for additional data to be sure that this range is actually met in nature; we will conclude that earthquakes within this predicted range are possible only if we are sure the model is in close agreement with a wide range of data.

(b) The P and S wave displacement spectra predicted by relaxation sources and partially verified by observations, are such that the P and S wave spectra have characteristic frequencies f_c^P and f_c^S which effectively divide the spectra into high and low frequency parts. The characteristic (i.e., corner or peak) frequencies are somewhat azimuth dependent and $f_c^S < f_c^P$ generally, although this relationship can be reversed in some azimuths. The behavior at high frequency $f > f_c^P$ (or f_c^S) is such that the average amplitude of the spectrum decreases rapidly from a maximum level at $f_c^P(f_c^S)$ reaching a mean slope proportional to $1/f^3$ for $f >> f_c^P(f_c^S)$. Superposed on this average behavior are secondary maxima and minima that are due to rupture propagation effects resulting in constructive and destructive inference. At low frequencies $f < f_c^P(f_c^S)$ the spectrum is even more complex in that both near and far field effects are present, and spectral shapes at long periods depend on the distance of the observation point from the source. The near field effects are dominated by terms which behave as $1/f$ at low frequency and this term can dominate within the entire range $f < f_c^P(f_c^S)$ at near source distances. At larger distances,the far field terms, having different distance dependence, dominate and the spectral behavior of this far field component is dependent on the dimensions of the prestress region. In particular, the spectrum is flat to zero frequency if the prestress region is taken to be infinite (which is impossible in the earth, of course), and decreases for $f << f_c^P(f_c^S)$ for the prestress region finite with a slope of f^2 for f small. For a small prestress

zone (prestressed zone dimension comparable to the rupture dimension) the spectrum is strongly peaked at $f_C^P(f_C^S)$ decreasing immediately toward the lower frequency end of the spectrum with the f^2 slope while for a larger prestress zone dimension, the peak broadens and as the prestress zone increases the peak continuously broadens being essentially flat until a frequency near $f_C'^R(f_C'^S)$ where it begins to decrease again with the f^2 slope. In general, the S wave spectra (either SV or SH) are from 5 to 10 times larger in magnitude than the P wave spectra and shifted somewhat to lower frequency but otherwise of similar overall shape.

(c) The spectral characteristics discussed in (b) above have been found, theoretically, to scale in a simple way. That is, a complete far field spectrum for an earthquake model, with failure parameters specified in terms of prestress magnitude and orientation $\sigma_{ij}^{(0)}$, fault or failure zone dimension L, rupture velocity V_R, intrinsic material velocities V_P and V_S, and relaxation zone or initial prestress zone "characteristic dimension" R_S; can be scaled to yield the spectra for any sized earthquake of similar type. These scaling laws appear to be in at least rough agreement with observations. The scaling law is as follows:

(1) The characteristic frequency for P waves:

$$f_C^P \alpha \ (L/V_R)^{-1}$$

In fact, f_C^P is essentially equal to V_R/L except that it varies somewhat with azimuth.

The characteristic frequency for S waves:

$$f_C^S \alpha \ (V_S/V_P) \ (L/V_R)^{-1}$$

Again f_C^S is very nearly equal to this quantity except for azimuthal variations which are somewhat larger than those for the P wave radiation (e.g. f_C^S can be larger than f_C^P at some azimuths).

(2) The spectral amplitude $|u_p|$ scales with rupture dimension L as:

$$|\tilde{u}_p| \ \alpha \ L^3$$

Similarly for S waves:

$$|\tilde{u}_s| \ \alpha \ L^3$$

The shape of the spectrum is not altered with changes in L, holding all other parameters fixed. (Note, however, that as L changes both f_C^P and f_C^S shift.)

(3) The spectral amplitudes scale directly with the prestress (or prestrain, $e_{ij}^{(0)}$ more properly), so:

$$|\tilde{u}_p| \ \alpha \ |e_{ij}^{(0)}| \quad \text{and} \quad |\tilde{u}_s| \ \alpha \ |e_{ij}^{(0)}|$$

(4) The width of the spectral peak (or flat portion of the spectrum which begins at f_C^P (or f_C^S for S waves) is controlled by R_S. The frequency $f_C^{'P}$ ($f_C^{'S}$) at which the spectrum falls off with decreasing f (as f^2) scales as:

$$f_C^{'P} \alpha (R_S/V_R)^{-1}$$

$$f_C^{'S} \alpha (V_S/V_P)(R_S/V_R)^{-1}$$

Therefore the spectral width of the peak (the flat portion of the spectrum is $\Delta f^P \cong f_C^P - f_C^{'P}$ or $\Delta f^S \cong f_C^S - f_C^{'S}$. Again the frequencies $f_C^{'P}$ and $f_C^{'S}$ appear to be nearly equal to the expressions given above (the factor of proportionality is nearly unity but varies with azimuth somewhat).

(d) The radiation patterns for P and S waves correspond to superposed multipole patterns, but the quadrupole is dominant at all frequencies (double couple force equivalent). However, at high frequencies the higher order multipoles became significant and the resulting observed patterns are distorted quadrupole (4 lobe) patterns, usually with high amplitudes in the direction of rupture propagation. These high frequency effects are due to rupture propagation (moving source effects). The patterns are nearly pure quadrupole at frequencies less than f_C^P and f_C^S.

In view of the previously summarized results, we considered the implications of these source properties insofar as discrimination was concerned. The discriminates considered in some detail so far were m_b vs. M_s, and P wave spectral shapes. The m_b - M_s results for earthquake can be summarized as follows:

(a) m_b and M_s were estimated using the log of the P wave amplitude at 1 cps for m_b and the log of the SV amplitude at .05 cps for M_s. One standard event was computed and the scaling laws previously described

were used to obtain results for larger and smaller events. (This will be replaced later by actual time domain measurements using synthetic seismograms generated from the spectra, and employing the actual field procedure followed in obtaining m_b and M_s). For earthquakes the m_b vs. M_s curve had a one to one slope at low magnitudes. Because of the expected variations in prestress and dimensions of the zone of prestress we actually obtain a band in the m_b - M_s plane within which earthquakes should occur. The band width is about one unit on the (vertical) M_s scale. The band then has the 45 degree slope in the m_b - M_s plane. Further at m_b magnitudes which appear to correspond to from 5^+ to 6.5^+, the curve quite abruptly becomes vertical indicating a maximum m_b of around 6.5. Larger fault lengths involving larger earthquakes will not give m_b any larger than about 6.5. But with very high prestress of the order of kilobars, this maximum m_b could be as high as 7. The curve (or band more properly) continues upward until at around M_s of 11, it terminates. (No earthquake, however great in length, would have a larger M_s than 11, for M_s measured in this way.) The fault lengths corresponding to the critical points for earthquake m_b vs. M_s are near 10 km (for the m_b cutoff) and near 900 km (for the M_s and m_b cutoff or termination point). The earthquake population should lie in a band of one magnitude unit (roughly) and this arises from the possible variations among earthquakes of the rupture velocity, the prestress, and dimension of the prestress zone.